



Cite this: *Phys. Chem. Chem. Phys.*, 2019, 21, 25606

Electronic couplings and rates of excited state charge transfer processes at poly(thiophene-co-quinoxaline)–PC₇₁BM interfaces: two- versus multi-state treatments†

Tuuva Kastinen, ^a Demetrio Antonio da Silva Filho, ^b Lassi Paunonen, ^c Mathieu Linares, ^{def} Luiz Antonio Ribeiro Junior, ^b Oana Cramariuc ^{gh} and Terttu I. Hukka ^a

Electronic coupling between adjacent molecules is one of the key parameters determining the charge transfer (CT) rates in bulk heterojunction (BHJ) polymer solar cells (PSCs). We calculate theoretically electronic couplings for exciton dissociation (ED) and charge recombination (CR) processes at local poly(thiophene-co-quinoxaline) (TQ)–PC₇₁BM interfaces. We use eigenstate-based coupling schemes, *i.e.* the generalized Mulliken–Hush (GMH) and fragment charge difference (FCD) schemes, including 2 to multiple (3–11) states. Moreover, we study the effects of functionals, excited state methods, basis sets, surrounding media, and relative placements of TQ and PC₇₁BM on the coupling values. Generally, both schemes provide consistent couplings with the global hybrid functionals, which yield more charge-localized diabatic states and constant coupling values regardless of the number of states, and so the 2-state schemes may be sufficient. The (non-tuned and optimally tuned) long-range corrected (LRC) functionals result in more notable mixing of the local components with the CT states. Employing multiple states reduces the mixing and thus improves the LRC results, although the method still affects the GMH CR couplings. As the FCD scheme is less sensitive, we recommend combining it with the multi-state treatment for polymer–fullerene systems when using the LRC functionals. Finally, we employ the 11-state FCD couplings to calculate the ED and CR rates, which are consistent with the experimental rates of the polymer–fullerene systems. Our results provide more insight into choosing a suitable eigenstate-based coupling scheme for predicting the electronic couplings and CT rates in photoactive systems.

Received 31st August 2019,
Accepted 31st October 2019

DOI: 10.1039/c9cp04837e

rsc.li/pccp



^a Chemistry and Advanced Materials, Faculty of Engineering and Natural Sciences, Tampere University, FI-33014 Tampere University, P. O. Box 541, Finland.

E-mail: tuuva.kastinen@tuni.fi, tertu.hukka@tuni.fi

^b Institute of Physics, University of Brasília, Brasília, DF, Brazil

^c Mathematics, Faculty of Information Technology and Communication Sciences, Tampere University, FI-33014 Tampere University, P. O. Box 692, Finland

^d Laboratory of Organic Electronics, ITN, Campus Norrköping, Linköping University, SE-581 83 Linköping, Sweden

^e Scientific Visualization Group, ITN, Campus Norrköping, Linköping University, SE-581 83 Linköping, Sweden

^f Swedish e-Science Research Centre (SeRC), Linköping University, SE-581 83 Linköping, Sweden

^g Physics, Faculty of Engineering and Natural Sciences, Tampere University, FI-33014 Tampere University, P. O. Box 692, Finland

^h Centrul IT pentru Stiinta si Tehnologie, Av. Radu Beller 25, Bucharest, Romania

† Electronic supplementary information (ESI) available: Additional information regarding the TQ–PC₇₁BM models and the methods; the excited state properties of the isolated TQ and PC₇₁BM models and the corresponding complexes investigated with B3LYP and CAM-B3LYP; the OT ω for the isolated TQ and PC₇₁BM models and the 3T4Q–PC₇₁BM/3Q4T–PC₇₁BM complexes; vertical excitation energies, and adiabatic and diabatic $\Delta\mu$ and Δq values for the CT₁ and LE states; NTOs of 3T4Q–PC₇₁BM, and electronic couplings of 3T4Q–PC₇₁BM and 3Q4T–PC₇₁BM; and bond length alternations of 3T4Q and 3Q4T. See DOI: [10.1039/c9cp04837e](https://doi.org/10.1039/c9cp04837e)

Introduction

Polymer solar cells (PSCs), which consist of conjugated donor–acceptor (D–A) copolymers as electron donor (eD) materials, have recently reached power conversion efficiencies (PCEs) up to 12%^{1,2} when using a fullerene derivative, *e.g.* PC₇₁BM (phenyl-C₇₁-butyric acid methyl ester), as an electron acceptor (eA) material. In recent years, PCEs up to 13–14%^{3,4} have been achieved with non-fullerene materials as the eAs. These best performing PSCs make use of a bulk heterojunction (BHJ) architecture⁵ in the photoactive layer, where the eD is mixed with the eA, ensuring the closest contact and an efficient charge transfer (CT) between the eD and eA materials.

Charge generation at the eD–eA interface is based on photo-induced electron transfer (PET), whose efficiency is determined by the following CT processes^{6,7} (Fig. 1a): (i) absorption of light by the eD (or the eA in some cases) leading to the formation of a locally excited state (LE, *i.e.* eD*–eA) and excitons (*i.e.* coulombically bound electron–hole pairs); (ii) diffusion of excitons to the eD–eA interface; (iii) exciton dissociation (ED) *via* an

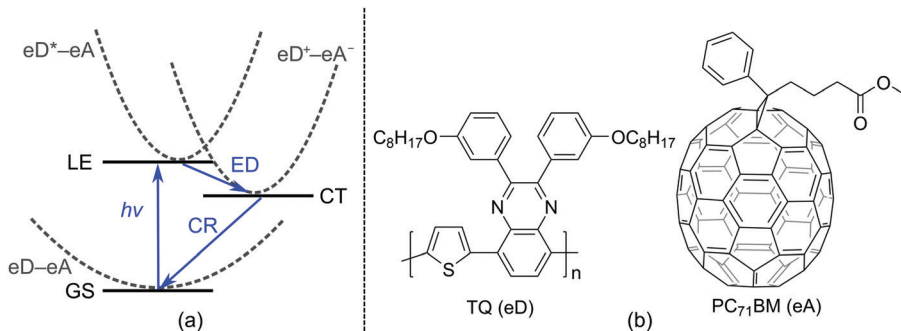


Fig. 1 (a) Schematic energy diagram illustrating the main steps of the photophysical processes occurring in the photoactive layer of a BHJ PSC. (b) Structures of an eD (TQ) and an eA (PC₇₁BM).

electron transfer from the eD* to eA and the formation of a CT state (eD⁺–eA[–]); (iv) if the charge carriers overcome the Coulomb binding energy, their separation into free carriers; and (v) migration of charges towards the electrodes. Alternatively, the CT state can decay *via* radiative emission or iridative charge recombination (CR) to the ground state (GS, *i.e.* eD–eA), which hinders the charge generation and thus reduces the performance of the device. Thus, maximizing the ED (and charge separation) rate and minimizing the CR rate are crucial for the efficiency of a PSC.

Predicting the rates of the ED and CR processes gives more insight into the efficiency of the charge generation at the eD–eA interface. In the high-temperature (weak-coupling), $k_B T \gg \hbar\omega$, regime, the semi-classical Marcus theory^{8–10} can be used to calculate the ED and CR rates:

$$k_{\text{ED/CR}} = \frac{|H_{\text{if}}|^2}{\hbar} \sqrt{\frac{\pi}{\lambda k_B T}} \exp\left[-\frac{(\Delta G^\circ + \lambda)^2}{4\lambda k_B T}\right], \quad (1)$$

where H_{if} is the electronic coupling (also referred to as a transfer integral) between the initial (i) and final (f) states of the CT process considered;¹¹ k_B and \hbar are the Boltzmann and reduced Planck constants, respectively; T is the temperature; λ is the reorganization energy (consisting of the inner, λ_i , and outer, λ_s , contributions, see the ESI†); and ΔG° is the Gibbs free energy. As the ED and CR rates are directly proportional to H_{if} , it is one of the key parameters determining them.⁷

The electronic coupling H_{if} describes the strength of the interaction between the initial and final charge-localized (diabatic) states. It is defined as the off-diagonal matrix element of the electronic Hamiltonian (H): $H_{\text{if}} = \langle \psi_i | H | \psi_f \rangle$, where ψ_i and ψ_f are the wave functions of the initial and final diabatic states of interest.¹¹ Thus, the value of H_{if} depends on the overlap of ψ_i and ψ_f and is very sensitive to the relative intermolecular position and distance of the eD and eA molecules.^{12,13} For this reason, an accurate estimation and prediction of the H_{if} values between the interacting species is a challenging subject of research in biology, chemistry, and physics.^{11,14}

Experimentally, H_{if} has been evaluated from spectroscopic data by fitting them into theoretical expressions.¹⁵ Theoretically, a number of computational methods based on *ab initio* quantum mechanics (QM) have been proposed and applied to

estimate the CT couplings.^{11,16,17} For calculating H_{if} of the CT processes involving excited states, *e.g.* ED and CR, different diabatization schemes have been developed. In these schemes, adiabatic states retrieved from QM calculations are transformed to diabatic states by using either the wave-function, as in the Boys localization,¹⁸ the Edmiston–Ruedenberg localization,¹⁹ and block diagonalization,^{20,21} or an additional operator, *e.g.* dipole moment (μ) in the generalized Mulliken–Hush (GMH)^{22,23} scheme or charge difference (Δq) in the fragment charge difference (FCD)²⁴ scheme. In addition, more simple approaches have been developed recently, where electronic couplings are obtained either directly²⁵ from excitation energies and oscillator strengths or by defining the quasi-diabatic states,²⁶ which are derived from the excited electronic states of the reference structures. In this paper, we will focus on the GMH and FCD schemes that are available in the Q-Chem software,²⁷ as they have proven to be useful and flexible for calculating electronic couplings for the excited state processes^{22,24,28} and they can be employed for large molecules, as well.¹⁶

Previously, a number of theoretical investigations have been reported using the two-state GMH and FCD schemes for determining H_{if} at local photoactive eD–eA interfaces, such as phthalocyanine–C₆₀,²⁹ pentacene–C₆₀,^{30–32} and D–A copolymer–fullerene systems.^{33–39} In particular, the two-state GMH scheme has been used in several studies of D–A copolymers and fullerene derivatives.^{33–38} However, in these studies, mainly the electronic couplings between the GS and excited states, *i.e.* the CR couplings, have been taken into account,^{33–36} while there are fewer studies^{37,38} which consider the couplings between the excited states, *e.g.* the LE and CT states, in the case of the ED process. In the PET, all these states are relevant for describing the ED and CR processes at the copolymer–fullerene interfaces. Moreover, to the best of our knowledge the effectiveness of the FCD scheme for predicting H_{if} in these systems in comparison with the GMH scheme has not yet been studied, and thus further information about this is required.

Typically, two eigenstates are included in the GMH and FCD calculations to form charge-localized diabatic states. However, previous studies of the complexes consisting of small or medium sized organic molecules,^{28,40,41} DNA π stacks,^{24,42–44} donor–bridge–acceptor systems,^{28,45} and TiO₂–dye systems⁴⁶ have shown that sometimes several adiabatic states are necessary



to describe the diabatic states accurately. In such instances, the corresponding multi-state GMH and FCD approaches are required.^{28,40} This is commonly the case, for example, when the component of the local excitation of the eD or eA is mixed with the CT state, and the two-state GMH scheme may lead to overestimated electronic coupling values.⁴⁷ However, to our knowledge, there are not yet studies which take account of the multi-state effects when predicting the coupling values with either the GMH or FCD scheme for the photoactive components of the active layers in PSCs containing D-A copolymers.

Previous studies have shown^{48,49} that electronic couplings are sensitive to the choice of density functional theory (DFT). Global hybrid functionals with a fixed, global fraction of explicit Hartree–Fock (HF) exchange, including especially B3LYP,^{50,51} have been generally a popular choice in the theoretical studies of photovoltaic compounds, but they are known to tend to overdelocalize the electron density due to the many-electron self-interaction error (MSIE).^{52,53} However, among the global hybrids, PBE0,^{54–56} which is mainly based on fundamental constants rather than on fitting to empirical parameters, has been demonstrated to produce relatively accurate electron densities for a set of atomic species⁵⁷ and also for larger organic molecules with two to ten heavy atoms (e.g. carbon, oxygen, nitrogen, and sulfur).⁵⁸ Long-range corrected (LRC) functionals, where the exchange term in the Kohn–Sham energy functional is partitioned into short-range (SR) and long-range (LR) components by employing a splitting function (e.g. the standard error function or its extended versions⁵⁹), have resulted in improved excitation energies of copolymers and copolymer–fullerene systems with respect to B3LYP.⁵³ In LRC functionals, DFT exchange is used for the SR part to treat the SR static correlation effects, while semilocal correlation is used for the LR part together with the full (100%) HF exchange, which will ensure the correct description of the asymptotic potential.⁵³ In particular, the LRC functional CAM-B3LYP⁶⁰ has been employed to reveal the excited state properties in the previous GMH coupling and CT rate calculations of copolymer–fullerene systems.^{33–36} However, here we note that not all functionals based on the range separation formalism actually include the full HF exchange, CAM-B3LYP with the 65% HF exchange in the LR component being one example, which may have consequences on the predicted values.⁶¹ In LRC functionals, the amount of (de)localization error is dependent on the range-separation parameter (ω), which defines the switching between the SR and LR. As ω is system-dependent,⁶² using the default ω values can lead to inaccurate results, and thus to address the problem of the MSIE, optimally tuned (OT) LRC functionals have been introduced.⁵³ Tuning of ω in the LRC functionals is known to improve the calculated excitation energies of D–A copolymers with respect to the experimental ones.^{63–66} Moreover, the FCD scheme has been reported to yield electronic couplings of stacked small molecules (*i.e.* ethylene, pyrrole, and naphthalene) closer to the experimental Mulliken–Hush values, when the OT version of the LRC Baer–Neuhauser–Livshits (BNL)^{67,68} functional

(incorporating the full 100% HF exchange into the LR component) has been used.⁴⁹

In the present work, we calculate the electronic couplings of the ED and CR processes at local polymer–fullerene interfaces with two- and multi-state GMH and FCD schemes. For our model systems of the eD–eA interfacial complexes, we have chosen to use a D–A copolymer, poly[thiophene-2,5-diyl-*alt*-2,3-bis-(3-octyloxyphenyl)quinoxaline-5,8-diyl]^{69,70} (TQ, Fig. 1b), as the eD and a fullerene derivative, PC₇₁BM,⁷¹ as the eA. These photoactive components have been widely used in BHJ PSCs, demonstrating promising efficiencies and high open-circuit voltages,⁷² making them a representative model system for this study. In particular, TQ has several interesting characteristics such as being an easily synthesized copolymer with a low bandgap, whose solubility and twisting can be effectively controlled with different side chains.^{70,73} Recently, TQ and its fluorinated counterparts have been employed successfully as the eDs also in all-polymer solar cells.⁷⁴ Furthermore, from a theoretical point of view, a small size of TQ allows using suitably long oligomers in the complex systems, while maintaining small enough systems in the computationally heavy time-dependent (TD) DFT calculations.

Our purpose is to determine how the inclusion of multiple states affects the GMH and FCD couplings of relatively large photovoltaic complexes. Additionally, we consider the performance of the aforementioned coupling schemes relative to the choice of functional, excited state method, basis set, and surrounding medium. We have selected a small series of representative functionals, namely two global hybrid functionals, B3LYP and PBE0, and two LRC functionals, (non-tuned) CAM-B3LYP and OT-BNL, which we have chosen based on the reasons presented above. As the tuning of ω in the LRC functionals is known to improve results for the polymer–fullerene systems with respect to the global hybrid and non-tuned LRC functionals (see above), we pay close attention to the performance of the tuned LRC functional with respect to the other selected functionals. Finally, we calculate the rates for the ED and CR processes at two TQ–PC₇₁BM interface configurations, where PC₇₁BM locates on either the D or A unit of TQ. Our findings provide insight into choosing the electronic coupling schemes for these types of eD–eA systems used in PSCs.

Computational details

Models

Two different series of TQ–PC₇₁BM complexes were constructed using the separately optimized B3LYP GS geometries of the (neutral) TQ oligomers and PC₇₁BM (the α isomer⁷¹): one, where PC₇₁BM was on top of the middle thiophene (the D unit) of TQ, and another, where PC₇₁BM was on top of the middle quinoxaline (the A unit) of TQ (see the ESI[†] for more detailed information about the models). The alkoxyphenyl side groups of the TQ oligomers (Fig. 1b) were replaced with hydrogens to reduce the computational cost and to ensure planar backbones. Because the DFT-based methods, *e.g.* TDDFT, set restrictions to



the sizes of the eD-eA complexes, we modeled the TQ oligomers with several lengths to choose the TQ models that would best represent the polymeric limit in the electronic coupling calculations. We note that the studied complexes present only two options for the possible placements of PC₇₁BM on TQ that can exist in real solution or thin film environments. Although the face-on configurations (*i.e.* PC₇₁BM on top of TQ) can be expected to yield larger electronic couplings than the edge-on configurations (*i.e.* PC₇₁BM on the side of TQ),^{39,75,76} there might be a relative positioning of the compounds different from the ones used here that yields the maximum electronic coupling between them. The intermolecular distance between TQ and PC₇₁BM (d , Fig. 2a) was set at 3.5 Å, which is an average we predicted in our previous study for poly(benzodithiophene-*co*-quinoxaline)-PC₇₁BM complexes with functionals including long-range and dispersion corrections.⁶⁶ The same intermolecular distance has also been employed in other theoretical polymer–fullerene interface studies.^{34,77} The distances between the centers of mass ($R_{\text{eD-eA}}$, Fig. 2a) of TQ and PC₇₁BM are *ca.* 8.6 Å.

Methods

We carried out the DFT and TDDFT calculations using the Q-Chem 4.2 software.²⁷ The medium was taken into account, as specified later. The GS geometries of the isolated models of the neutral TQ oligomers and PC₇₁BM and their radical states (cations for TQ and anions for PC₇₁BM; only for the longest TQ oligomers, see the ESI†) were fully optimized in vacuum using DFT with the global hybrid functional B3LYP and the 6-31G** basis set. Moreover, the geometries of the lowest singlet excited (S_1) of the longest TQ oligomers were optimized with TDDFT at the same level of theory. In all the geometry

optimizations, the fine grid EML(75,302) with 75 Euler–Maclaurin radial grid points⁷⁸ and 302 Lebedev angular grid points,⁷⁹ an SCF convergence criterion of 10^{-9} , and a cutoff for neglect of two electron integrals of 10^{-14} were employed. In the single point (SP) calculations of the isolated compounds related to the excited state, reorganization energy, and Gibbs free energy calculations and those of the selected complexes (Fig. 2b) related to the excited state and electronic coupling calculations, the 6-31G* basis set, the standard SG-1 grid, and the default values for the SCF convergence (10^{-5}) and cutoff of two electron integrals (10^{-8}) were used, unless stated otherwise. The excited state SP energy calculations of both the isolated models and the complexes were carried out for the lowest 10 singlet excited states with both the full TDDFT and TDA-DFT schemes, incorporating the Tamm–Dancoff approximation (TDA)⁸⁰ in the latter. We note that sometimes ED and CR processes may involve triplet states,⁸¹ but here we have concentrated on those including only singlet states. B3LYP and the LRC functional CAM-B3LYP (with the default range-separation parameter, ω , of 0.33 Bohr⁻¹) were used in all SP calculations. Additionally, the global hybrid functional, PBE0, and the OT version of the BNL LRC functional (OT-BNL) were used in the SP calculations of the selected TQ–PC₇₁BM complexes (see ‘Models’ and ‘Length of the TQ oligomer and the polymeric limit’). The OT ω values (originally 0.5 Bohr⁻¹) for the selected TQ–PC₇₁BM complexes were determined using eqn (S1) and the tuning procedure is presented in the ESI.† We note that, in addition to the tuning of ω , incorporation of some amount of HF exchange in the SR component has been observed to improve the prediction of the optoelectronic properties of several aromatic heterocycles,⁸² DNA nucleobase compounds and their complexes,⁶¹ and compounds employed in organic

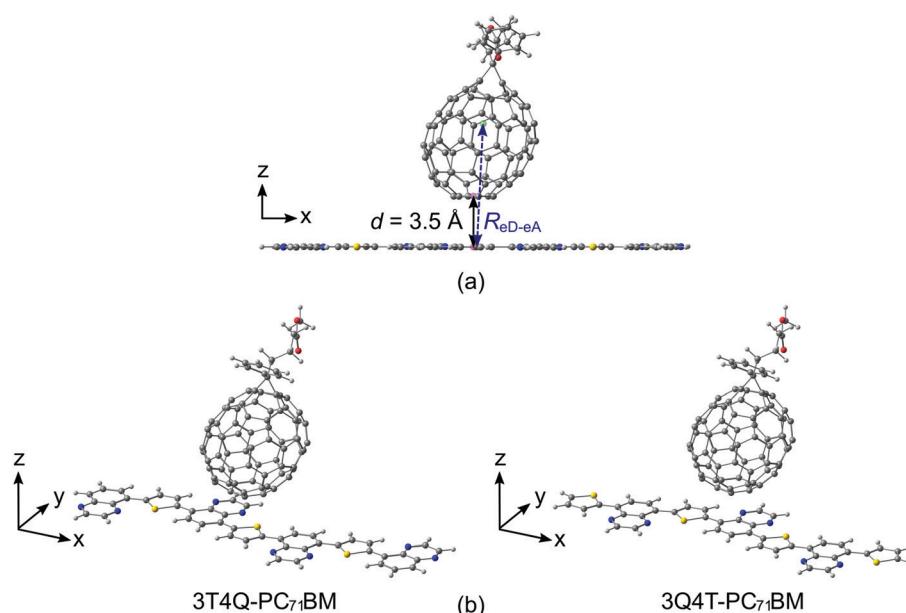


Fig. 2 Illustration of (a) intermolecular distance, d , and effective separation, $R_{\text{eD-eA}}$, between TQ and PC₇₁BM in the studied TQ–PC₇₁BM complexes. These distances were determined between the specified centroids, pink spheres for d , and the centers of mass, green spheres for $R_{\text{eD-eA}}$. (b) TQ–PC₇₁BM complexes with the longest TQ oligomer models, where PC₇₁BM is either above thiophene (3T4Q) or quinoxaline (3Q4T).



light emitting diodes.⁵⁹ The BNL functional we employ here does include only the LR HF exchange, but due to the extent of the various theoretical aspects studied here, we have chosen to concentrate only on the effect of the ω tuning in this study. Pictorial representations of the geometries and natural transition orbitals (NTOs)⁸³ were generated using ChemCraft 1.8.⁸⁴ The contributions of the electron densities of TQ and PC₇₁BM to the NTOs were determined with the C-squared Population Analysis (C-SPA).⁸⁵

Furthermore, we checked the role of the basis set and surrounding medium in the electronic couplings. We employed, besides 6-31G*, also 6-31G** and 6-31+G* with TDDFT and the B3LYP functional, and 6-31G** with the PBE0, CAM-B3LYP, and OT-BNL functionals. As these calculations were too heavy for the studied complexes, we were unable to verify the effect of 6-31+G* with the LRC functionals and the effect of any larger basis sets. Nor did we consider the other types of basis sets (*e.g.* Dunning's) here. The influence of the medium was taken into account in the coupling and CT rate calculations by means of the conductor-like polarizable continuum model (CPCM)^{86,87} with a Switching/Gaussian (SWIG) implementation⁸⁸ without geometry optimizations. Two different polarized media were considered: (i) a solvent with the static (ϵ_s) and dynamic (optical, ϵ_{op}) dielectric constants of 10.1210 and 2.4072 for 1,2-dichlorobenzene (1,2-DCB, at 293.15 K),⁸⁹ respectively, and (ii) a blend, *i.e.* a film with ϵ_s and ϵ_{op} of 3.6000⁹⁰ and 3.2761, respectively. The ϵ_{op} of the blend was calculated⁷⁷ by $\epsilon_{op} = n^2$ from the experimental refractive index (n) of the TQ-PC₇₁BM blend (*ca.* 1.81 at 532 nm).⁹¹

For determining the electronic couplings, we used both the GMH^{22,23} and FCD²⁴ schemes as implemented in Q-Chem 4.2²⁷ to calculate the adiabatic electronic (μ_{ii}^{ad}) and transition dipole moments (μ_{ij}^{ad}) (within the GMH scheme) and the charge differences (Δq_{ii}^{ad} and Δq_{ij}^{ad} , within the FCD scheme) for the GS and ten lowest singlet excited states. Among these 11 adiabatic states, the relevant states for the ED and CR processes, *i.e.* the GS [eD-eA], the LE state of TQ [eD*-eA], and the lowest CT state [CT₁, eD⁺-eA⁻] (Fig. 1), were assigned on the basis of the μ_{ii}^{ad} and Δq_{ii}^{ad} values and the NTOs (for more details see 'Assignment of the states' in the ESI†). The electronic couplings (eqn (S2)-(S11), ESI†), reorganization energies (eqn (S12)-(S18), ESI†), and Gibbs free energies (eqn (S19)-(S22), ESI†) for the ED and CR processes were calculated using the equations presented in the ESI†. The CT rates for the ED and CR processes were calculated with the Marcus theory (eqn (1)) at a temperature of 293.15 K. The 11-state FCD H_{if} values (eqn (S2)-(S4) in the ESI†) were used in the CT rate calculations.

Results and discussion

Length of the TQ oligomer and the polymeric limit

To select the TQ model that best represents the polymeric limit in the electronic coupling and CT rate calculations, we have studied the effect of the TQ length on the excited state properties of the isolated TQ models and the TQ-PC₇₁BM complexes (Fig. S1, ESI†). The results apply to both the B3LYP and

CAM-B3LYP functionals used in these calculations unless stated otherwise (see the ESI† for more detailed information). In general, both the T- and Q-series follow similar trends (Tables S1-S3, ESI†). The S₁ energies of the isolated TQ oligomers with the corresponding lengths are almost equal (Table S1, ESI†): the singlet energies decrease only slightly, when the chain length increases, as expected.^{28,40,45} The placement of PC₇₁BM, *i.e.* above either the central T or Q unit of the TQ oligomer, has a negligible or a very small effect on the excited state energies and oscillator strengths in the complexes of the T- and Q-series with the corresponding lengths (Tables S2 and S3, ESI†). In contrast, the energies of the main vertical excitation ($E_{vert,main}$, *i.e.* the excitation having the largest oscillator strength) and the CT₁ state decrease (the peaks red-shift), and the oscillator strengths of the peaks increase (except for the CT₁ state with CAM-B3LYP), when the length, and, therefore, the contribution of the TQ oligomer, increases in the complex. In the complexes with the shortest TQs, only local excitations of PC₇₁BM (LF) are observed and no LE or CT states are predicted (Tables S2 and S3, ESI†) within the ten lowest singlet excited states. The oligomers consisting of five units, *i.e.* 3T2Q and 3Q2T, are long enough for the LE and CT states to appear in the complexes, with LE being the main excitation. However, we have selected the complexes with the longest oligomers consisting of seven units, *i.e.* 3T4Q-PC₇₁BM and 3Q4T-PC₇₁BM, for the further calculations, as they have even more distinguishable LE and CT₁ states with both B3LYP and CAM-B3LYP. Foremost, the B3LYP energies of the CT₁ (*ca.* 1.6 eV) and LE states (*ca.* 1.9 eV) of 3T4Q-PC₇₁BM and 3Q4T-PC₇₁BM are closest to the experimental excited state energies ($E_{CT} = 1.4-1.5$ eV^{92,93} and $E_{LE} = 1.97$ eV taken from the absorption maximum in the experimental UV-Vis absorption spectrum of a TQ-PC₇₁BM (3:1) film⁹³). For the aforementioned reasons, 3T4Q-PC₇₁BM and 3Q4T-PC₇₁BM are expected to be our best candidates for further modeling of the properties of the TQ-PC₇₁BM complexes.

Effect of the functional on the excited state characteristics and electronic couplings

The functional has a clear effect on the excited state characteristics (*i.e.* excitation energies and nature of the state) of the studied complexes, 3T4Q-PC₇₁BM and 3Q4T-PC₇₁BM (Fig. 2b). Generally, when considering the 10 lowest adiabatic states of the complexes obtained with TDDFT (in vacuum), the excitation energies for the S₁-S₁₀ states increase in the order B3LYP (20% HF) < PBE0 (25% HF) < OT-BNL (with an OT ω of 0.17 Bohr⁻¹, see Table S4, ESI†) < CAM-B3LYP (Table S5, ESI†). The global hybrids B3LYP and PBE0 predict the three lowest excited states as the CT states, whereas the fourth state is the intramolecular excitation of TQ, *i.e.* the LE state. This ordering of the CT₁ and LE states, *i.e.* the CT₁ state is lower in energy than the LE state, is consistent with the experimental results^{92,93} (see above). Above the CT₁ and LE states in energy, the global hybrids predict local excitations of PC₇₁BM, *i.e.* the LF states, and higher-energy CT states, whose nature ('pure' *vs.* partial CT) and number (between one and three) vary somewhat regarding



the functional and position of PC₇₁BM on TQ. With the LRC functionals, CAM-B3LYP and OT-BNL, the order of the CT₁ and LE states is reverse, *i.e.* the CT₁ state is higher in energy (the fifth or sixth state) than the LE state (the second excited state in the most cases), which is in contrast to the results given by the global hybrids and experiments.^{92,93} Additionally, the LRC functionals predict fewer CT states among the calculated 10 lowest adiabatic excited states than the global hybrids.

These differences in the tendencies between the global hybrid and LRC functionals to predict the ordering of the states of polymer–fullerene complexes have been previously observed also for other systems by us⁶⁶ and others.⁸¹ Moreover, Zheng *et al.* observed the same ordering of the CT₁ and LE states also for pentacene–C₆₀ complexes⁹⁴ when using the OT LRC ωB97X-D and BNL functionals. Zheng *et al.* noticed that the OT values of ω are smaller when using PCM compared to those obtained in vacuum. Moreover, the energy of the CT₁ state is affected by ω and decreases with decreasing ω , eventually locating at an energy lower than that of the LE state. However, in their recent paper, Kronik and Kümmel pointed out⁹⁵ that including the PCM in the tuning of ω may lead to inconsistent results, as the PCM affects the total energies but not the DFT eigenvalues, resulting in the OT ω values that are notably smaller than those in vacuum. Thus, we have used the OT ω of OT-BNL obtained under vacuum also in the 1,2-DCB and blend environments explained later.

The functional has a notable effect on the nature of the adiabatic CT₁ state of the studied complexes, whereas the nature of the LE state is very similar regardless of the functional. The global hybrid functionals predict almost negligible mixing of the local states with the adiabatic CT₁ state, which is observed from the adiabatic $\Delta q_{ii}^{\text{ad}}$ values of the CT₁ state (*i.e.* $\Delta q_{\text{CT}1}^{\text{ad}}$ of 1.9–2.0 in Tables 1 and 2) as they are already close to the ideal value of 2.²⁸

Table 1 Adiabatic and diabatic electric dipole moments ($\Delta\mu_{ii}^{\text{ad}}$ and $\Delta\mu_{ii}^{\text{diab}}$)^a and charge differences ($\Delta q_{ii}^{\text{ad}}$ and $\Delta q_{ii}^{\text{diab}}$) for the CT₁ and LE states of 3T4Q–PC₇₁BM calculated with the 2–11-state GMH and FCD schemes^b using TDDFT and the 6-31G* basis set

Scheme		GMH				FCD			
Functional	N^c	$\Delta\mu_{\text{CT}1}^{\text{ad}}$	$\Delta\mu_{\text{CT}1}^{\text{diab}}$	$\Delta\mu_{\text{LE}}^{\text{ad}}$	$\Delta\mu_{\text{LE}}^{\text{diab}}$	$\Delta q_{\text{CT}1}^{\text{ad}}$	$\Delta q_{\text{CT}1}^{\text{diab}}$	$\Delta q_{\text{LE}}^{\text{ad}}$	$\Delta q_{\text{LE}}^{\text{diab}}$
B3LYP	2	31.0	31.0	1.1	0.6	1.9	1.9	0.1	0.1
	3		31.6		0.5		2.0		0.1
	4		31.4		0.5		2.0		0.1
	11		31.2		0.3		2.0		0.0
PBE0	2	29.9	30.0	1.4	0.7	1.9	1.9	0.1	0.1
	3		30.6		0.7		2.0		0.1
	4		30.5		0.7		2.0		0.1
	11		30.2		0.2		2.0		0.0
CAM-B3LYP	2	12.5	12.5	1.3	1.1	0.7	0.7	0.1	0.0
	3		13.6		0.2		0.8		0.0
	4		19.4		0.1		1.5		0.0
	11		26.6		0.6		1.9		0.0
OT-BNL	2	11.3	11.4	1.7	2.1	0.7	0.7	0.2	0.0
	3		13.5		0.4		0.8		0.0
	4		20.1		0.5		1.6		0.0
	11		24.5		0.3		1.8		0.0

^a Relative to the GS. ^b Values calculated in vacuum. ^c Number of the states.

Table 2 Adiabatic and diabatic electric dipole moments ($\Delta\mu_{ii}^{\text{ad}}$ and $\Delta\mu_{ii}^{\text{diab}}$)^a and charge differences ($\Delta q_{ii}^{\text{ad}}$ and $\Delta q_{ii}^{\text{diab}}$) for the CT₁ and LE states of 3Q4T–PC₇₁BM calculated with the 2–11-state GMH and FCD schemes^b using TDDFT and the 6-31G* basis set

Scheme		GMH				FCD			
Functional	N^c	$\Delta\mu_{\text{CT}1}^{\text{ad}}$	$\Delta\mu_{\text{CT}1}^{\text{diab}}$	$\Delta\mu_{\text{LE}}^{\text{ad}}$	$\Delta\mu_{\text{LE}}^{\text{diab}}$	$\Delta q_{\text{CT}1}^{\text{ad}}$	$\Delta q_{\text{CT}1}^{\text{diab}}$	$\Delta q_{\text{LE}}^{\text{ad}}$	$\Delta q_{\text{LE}}^{\text{diab}}$
B3LYP	2	31.4	31.4	0.2	0.0	2.0	2.0	0.0	0.0
	3		31.6		0.0		2.0		0.0
	4		31.6		0.0		2.0		0.0
	11		31.4		0.1		2.0		0.0
PBE0	2	30.5	30.5	0.1	0.2	2.0	2.0	0.0	0.0
	3		30.7		0.1		2.0		0.0
	4		30.8		0.1		2.0		0.0
	11		30.7		0.3		2.0		0.0
CAM-B3LYP	2	16.6	16.6	0.8	0.8	1.1	1.1	0.1	0.0
	3		17.4		0.0		1.2		0.0
	4		21.8		0.0		1.6		0.0
	11		27.9		0.3		1.9		0.0
OT-BNL	2	15.9	15.9	0.6	1.3	1.1	1.1	0.1	0.0
	3		17.3		0.7		1.2		0.0
	4		21.6		0.7		1.7		0.0
	11		26.3		0.5		1.9		0.0

^a Relative to the GS. ^b Values calculated in vacuum. ^c Number of states.

This can be observed also from the NTOs of the two complexes (Fig. 3 and Fig. S2, ESI†), for which B3LYP and PBE0 predict a complete CT from TQ to PC₇₁BM, as the hole NTO localizes totally on TQ and the electron NTO on PC₇₁BM. Similarly, the adiabatic $\Delta\mu_{ii}$ values of the CT₁ state (*i.e.* $\Delta\mu_{\text{CT}1}^{\text{ad}}$ in Table 1) are rather large (29.9–31.4 D), although not close to the ideal dipole moments (41.1 D for 3T4Q–PC₇₁BM and 41.3 D for 3Q4T–PC₇₁BM, see the ESI†). The LRC functionals predict a partial CT character for the CT₁ state ($\Delta\mu_{\text{CT}1}^{\text{ad}}$ of 11.3–16.6 D and $\Delta q_{\text{CT}1}^{\text{ad}}$ of 0.7–1.1, Tables 1 and 2), *i.e.* mixing of the local LF states with the CT state. When considering the corresponding NTOs, it can be seen that the hole NTO of the CT₁ state localizes on both TQ and PC₇₁BM and the electron NTO on PC₇₁BM. In this case, 3T4Q–PC₇₁BM has somewhat larger mixing of a LF component with the CT state and thus a smaller amount of CT compared to 3Q4T–PC₇₁BM. For the LE state, the global hybrid and LRC functionals predict small adiabatic $\Delta q_{ii}^{\text{ad}}$ (*i.e.* $\Delta q_{\text{LE}}^{\text{ad}}$ of 0.0–0.1 in Tables 1 and 2) and $\Delta\mu_{ii}^{\text{ad}}$ values (*i.e.* $\Delta\mu_{\text{LE}}^{\text{ad}}$ of 0.1–1.7 D in Tables 1 and 2). The NTOs of the LE state of both complexes have the same shapes with all four functionals, *i.e.* both the hole and electron NTOs are delocalized along the TQ backbone, although the global hybrids yield slightly more delocalized descriptions compared to the LRC functionals. Additionally, OT-BNL predicts a small amount of CT mixed with the LE state. These differences between the global hybrid and (non-tuned and OT) LRC functionals in predicting the nature of the adiabatic states of polymer–fullerene complexes have been previously observed also by us⁶⁶ and others.⁸¹

The nature of the diabatic states of the complexes obtained with the 2–11-state GMH and FCD schemes is very similar to that of the adiabatic ones when employing the global hybrid functionals, whereas with the LRC functionals the diabatic states are more localized than the adiabatic states. With B3LYP and PBE0, the $\Delta\mu_{ii}^{\text{diab}}$ (GMH) and $\Delta q_{ii}^{\text{diab}}$ (FCD) values of the LE and CT₁ states do not differ much from the adiabatic values (Tables 1 and 2).



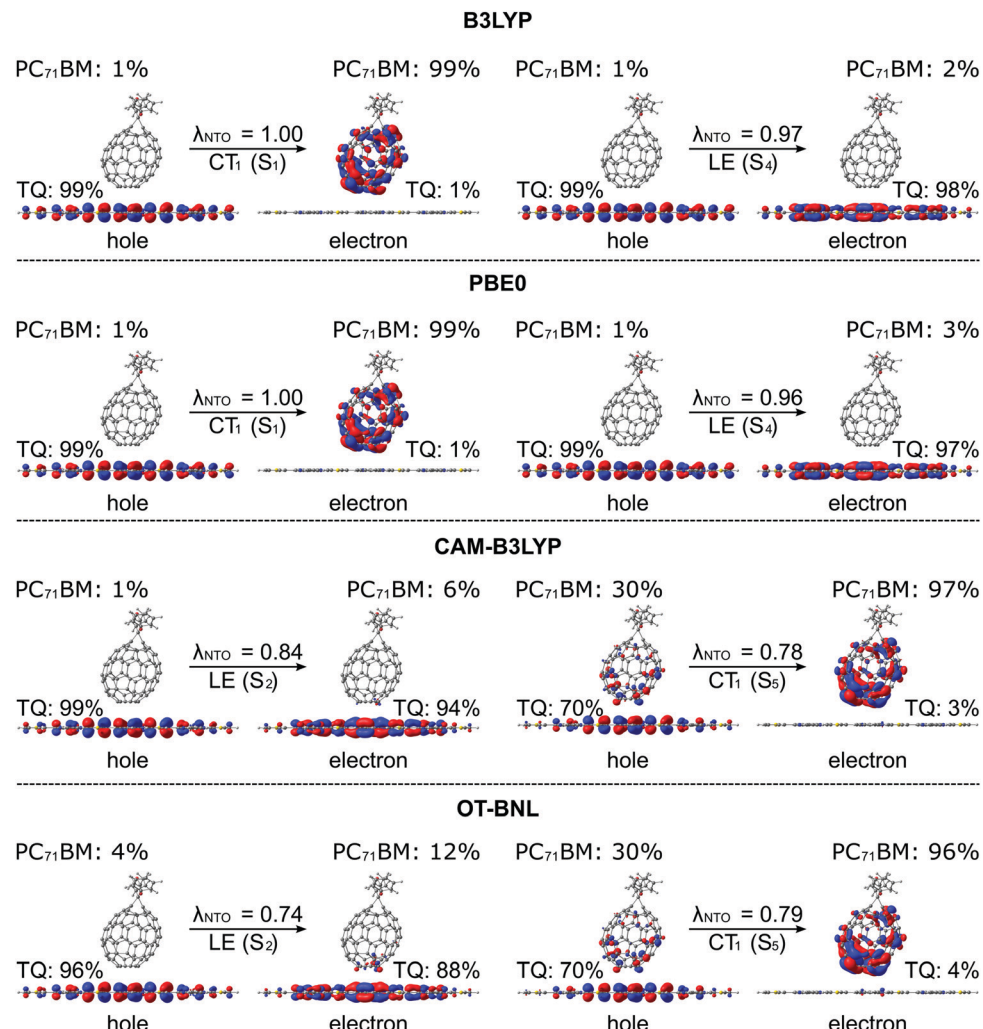


Fig. 3 NTOs (the main pair) corresponding to the CT_1 and LE states of the 3Q4T-PC₇₁BM complex calculated with TDDFT using different functionals and the 6-31G* basis set (isodensity contour = 0.025). Additionally, the contributions (%) of TQ and PC₇₁BM to the NTOs and contributions (λ_{NTO}) of the NTO pair to the particular state are presented.

This is most probably because the mixing of the states is small already for the adiabatic states, as mentioned above. The $\Delta q_{CT_1}^{\text{diab}}$ values predicted by the 2-11-state FCD schemes with the global hybrids mainly reach the ideal value of 2, indicating a complete CT from TQ to PC₇₁BM. However, the $\Delta \mu_{CT_1}^{\text{diab}}$ values calculated with the 2-11-state GMH schemes and the global hybrids are still smaller than the ideal dipole moments (41.1 D for 3T4Q-PC₇₁BM and 41.3 D for 3Q4T-PC₇₁BM). This might indicate that the number of states used here is not enough for generating more localized diabatic states in the GMH schemes and thus for reaching the ideal dipole moments. When employing the LRC functionals in the 2-11-state FCD schemes, the diabatization effectively removes the local components that are present in the CT_1 state, yielding $\Delta q_{CT_1}^{\text{diab}}$ values of 1.8–1.9, which are quite close to the ideal one. Similarly, the $\Delta \mu_{CT_1}^{\text{diab}}$ values, predicted with the 3-11-state GMH schemes and the LRC functionals, are now clearly larger than the adiabatic ones (Tables 1 and 2), although still not reaching the ideal dipole moments either. Thus, diabatization has a larger effect on the localization of the

CT_1 state with the (non-tuned and OT) LRC functionals compared to the global hybrids.

In most cases, all functionals predict that the 2-11-state CR electronic couplings calculated in vacuum are larger than the corresponding ED couplings (Tables S14 and S15, ESI†). However, when PC₇₁BM is above quinoxaline (the A unit) of TQ (3Q4T-PC₇₁BM), the LRC functionals predict mainly the opposite, *i.e.* larger ED couplings than the CR couplings with both the GMH and FCD schemes (except for the 11-state GMH scheme). The global hybrid functionals yield quite similar couplings (Fig. 4 and Fig. S3, ESI†), whereas the LRC functionals predict somewhat larger values (Fig. 5 and Fig. S4, ESI†). Overall, the ED couplings predicted with B3LYP and PBE0 for 3T4Q-PC₇₁BM and 3Q4T-PC₇₁BM are *ca.* 36–47 meV and 21–31 meV, respectively, whereas the CR couplings are *ca.* 43–56 meV and 25–34 meV, respectively. The ED couplings calculated with CAM-B3LYP and OT-BNL for 3T4Q-PC₇₁BM and 3Q4T-PC₇₁BM are *ca.* 49–83 meV and 33–56 meV, respectively, and the CR couplings are *ca.* 74–142 meV and 3–92 meV, respectively.



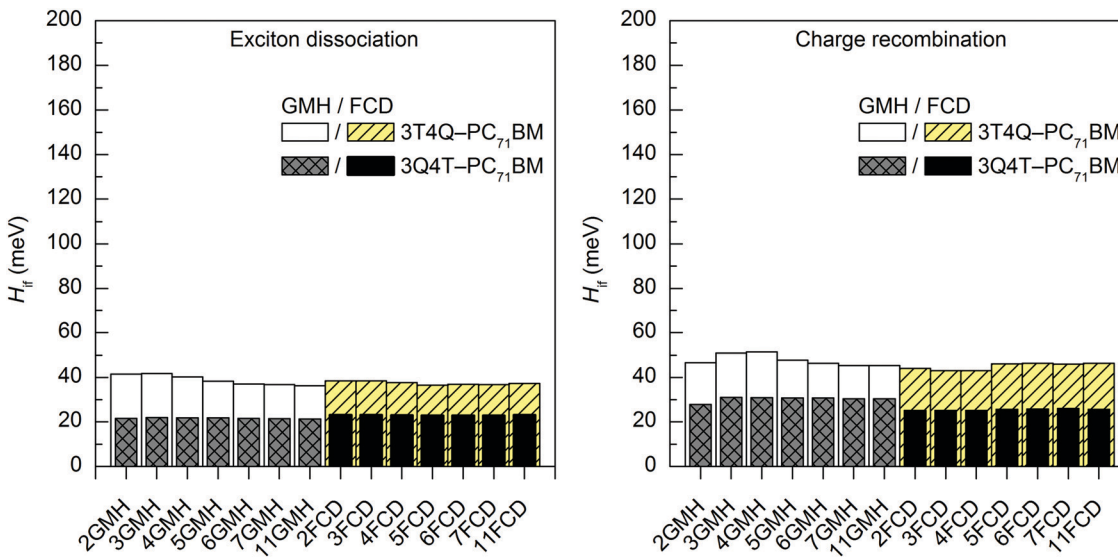


Fig. 4 Electronic coupling values of the studied TQ-PC₇₁BM complexes calculated with TDDFT at the B3LYP/6-31G* level of theory using the GMH and FCD schemes with different numbers of states (2–11).

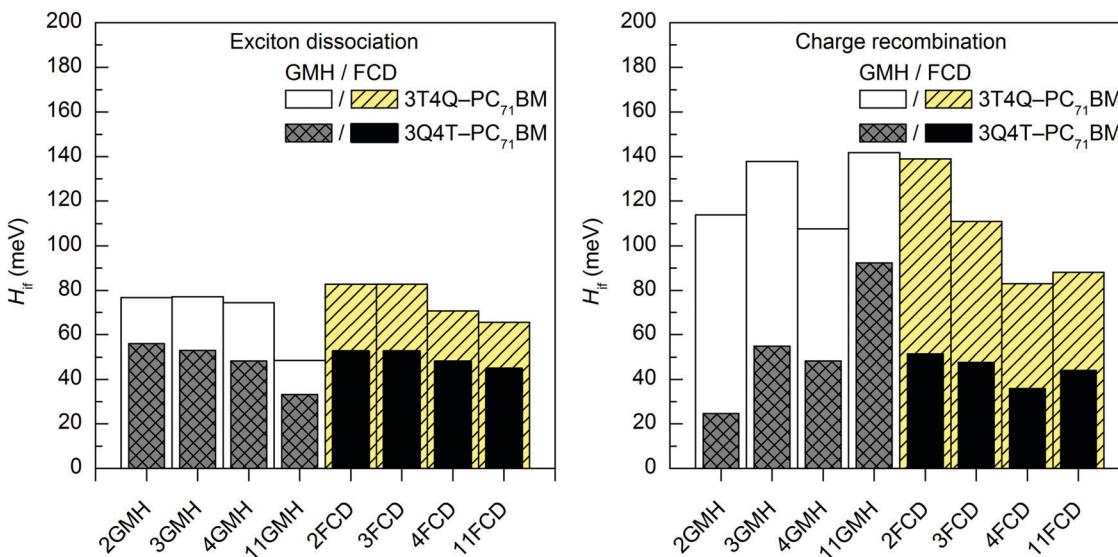


Fig. 5 Electronic coupling values of the studied TQ-PC₇₁BM complexes calculated with TDDFT at the OT-BNL/6-31G* level of theory using the GMH and FCD schemes with different numbers of states (2–11).

In general, the couplings increase in the order of B3LYP (20% HF) < PBE0 (25% HF) < CAM-B3LYP \leq OT-BNL. Sini *et al.* also noticed that the coupling values increase with the increasing amount of HF exchange⁴⁸ in their study of a tetra-thiafulvalene-tetracyanoquinodimethane complex with the direct coupling method.¹³ Even though we have not calculated the amounts of effective HF exchange⁴⁸ in CAM-B3LYP and OT-BNL for our complexes, as this would require a larger set of functionals with the known amounts of HF exchange, we expect that the electronic coupling value increases with the increasing amount of effective HF exchange in the functional.

To summarize, the functional has a notable effect on the excited state characteristics, *i.e.* the vertical excitation energies

and nature of the adiabatic and diabatic states, and therefore the electronic couplings. With the global hybrid functionals, both the adiabatic and diabatic CT₁ states have a similar, localized nature, *i.e.* a complete CT from TQ to PC₇₁BM. With the LRC functionals, local components mixed with the adiabatic CT₁ state are effectively removed by diabatization, especially with the FCD scheme. The couplings are larger with the LRC functionals than with the global hybrids.

Effect of the number of states on the electronic coupling values

The evolutions of the ED and CR electronic couplings of the selected complexes (in vacuum) with different numbers of states indicate that the functional has a clear effect on the

relationship between the coupling and the number of states (Fig. 4 and Fig. S3, ESI[†] for the global hybrids, and Fig. 5 and Fig. S4, ESI[†] for the LRC functionals). The corresponding numerical values are given in Tables S14 and S15, ESI[†]. With the global hybrid functionals, the number of states does not seem to have a very strong effect on the coupling values, as increasing the number of states decreases both the ED and CR couplings only slightly (by 0–5 meV) and they are rather constant with both the GMH and FCD schemes. This is most probably because the global hybrids predict small or negligible mixing of the adiabatic states for the studied TQ-PC₇₁BM complexes (see 'Effect of the functional on the excited state characteristics and electronic couplings' above), and the diabatization does not change the nature of the states much even with the increased number of states. This can be observed from the $\Delta\mu_{CT1}^{diab}$ and Δq_{CT1}^{diab} values (Tables 1 and 2), as they remain rather unchanged with an increasing number of states and are already close or equal to the ideal ones of 41.1 D and 41.3 D (for 3T4Q-PC₇₁BM and 3Q4T-PC₇₁BM, respectively) and of 2, respectively. Additionally, the GMH and FCD schemes yield quite similar coupling values when using the global hybrids, indicating that both schemes yield similar diabatic states.²⁸ Thus, with the global hybrids, the 2-state schemes seem to be sufficient for calculating the electronic couplings.

With the LRC-functionals (Fig. 5 and Fig. S4, ESI[†]), the electronic couplings of the studied complexes change more significantly with the number of states compared to the global hybrids. The GMH and FCD ED couplings predicted with the LRC functionals decrease with the increasing number of states, although in some cases the 3-state results are slightly higher than the 2-state results (Tables S14 and S15, ESI[†]). The 2–4-state GMH ED couplings are rather similar, whereas the 11-state values are notably smaller. With the FCD scheme, the ED couplings decrease in a more constant way. The GMH and FCD CR couplings oscillate somewhat with the increasing number of states. The GMH scheme predicts larger CR couplings with 11 states than with 2–4 states, whereas the FCD CR couplings mainly decrease when the number of states increases. Here, the tuning of ω does not seem to have a strong effect on the overall trends in the couplings, as both CAM-B3LYP and OT-BNL predict similar changes.

The number of states used here is restricted by the size of the systems and the computational time limit and therefore we are not able to judge whether the electronic couplings obtained with the LRC functionals have converged to certain values²⁸ already with 11 states or whether more states would improve the results. However, both the $\Delta\mu_{CT1}^{diab}$ and Δq_{CT1}^{diab} values increase with the increasing number of states (Tables 1 and 2). Moreover, even though the 11-state $\Delta\mu_{CT1}^{diab}$ values do not reach the ideal dipole moments of 41.1 D and 41.3 D (for 3T4Q-PC₇₁BM and 3Q4T-PC₇₁BM, respectively), they have improved compared to the 2–4-state values. Furthermore, the Δq_{CT1}^{diab} values are almost equal to the ideal value of 2. Thus, the 11-state GMH and FCD schemes can be expected to yield better descriptions of the diabatic states and the couplings than the 2–4 states, and for that reason, we have employed the 11-state GMH and FCD schemes in the further electronic coupling calculations.

Effect of the TD method on the excited state characteristics and the electronic couplings

Generally, the TD method does not seem to have any effect on the vertical excitation energies of the studied TQ-PC₇₁BM complexes, as both TDDFT and TDA yield almost identical values (in vacuum, Tables S5 and S6, ESI[†]). Next to equal excitation energies with both TD methods have also been observed for both small molecules⁸⁰ and large interfacial complexes (pentacene-C₆₀⁹⁴ and copolymer-fullerene⁹⁶) in previous studies. However, here we observe that the number of CT states and the ordering of the states are in some cases slightly different with TDDFT and TDA, especially with the LRC functionals, which seem to have an effect on the GMH electronic couplings (see below).

The nature of the adiabatic LE and CT₁ states does not change significantly with the TD method when employed together with the global hybrid functionals, as TDDFT and TDA yield similar $\Delta\mu_{ii}^{ad}$ and Δq_{ii}^{ad} values in most cases (Tables 1 and 2 and Table S13, ESI[†]). With the LRC functionals, TDA yields slightly larger (0.2–0.5) Δq_{CT1}^{ad} values and somewhat larger (2.8–4.5) $\Delta\mu_{CT1}^{ad}$ values than TDDFT; that is, the mixing of the LF component with the adiabatic CT₁ state is not as strong with TDA as with TDDFT. However, diabatization of the adiabatic states with the 11-state GMH and FCD schemes results mostly in similar $\Delta\mu_{CT1}^{diab}$ and Δq_{CT1}^{diab} values with both TDDFT and TDA for diabatic LE and CT₁ states.

Both TD methods yield very similar 11-state electronic couplings with the global hybrid functionals, with the difference between them being only 0–4 meV (Fig. 6 and 7 and Tables S14–S16, ESI[†]). In addition, the 11-state FCD couplings calculated with the LRC functionals are only moderately different (by 0–12 meV) when using either TDDFT or TDA. However, the 11-state GMH couplings obtained with TDDFT and TDA and the LRC functionals differ more, namely by 2–49 meV, with TDA predicting larger couplings in most cases. The largest differences between the two TD methods are in the GMH CR couplings, which is most probably due to the differences in the $\Delta\mu^{ad}$ values other than those of the CT₁ and LE states. The tuning of ω does not seem to have a clear effect, as overall both the non-tuned CAM-B3LYP and OT-BNL functionals predict the same trends. Overall, TDA predicts the same trends as TDDFT: mostly larger CR couplings than the ED couplings (and *vice versa* for some 11-state FCD results for 3Q4T-PC₇₁BM with the LRC functionals), larger ED and CR couplings for 3T4Q-PC₇₁BM than for 3Q4T-PC₇₁BM, and larger ED and CR couplings with the LRC functionals than with the global hybrids.

To conclude, for the studied TQ-PC₇₁BM complexes, TDA yields consistent results with TDDFT when using the global hybrids. Thus, as TDA is computationally less costly,⁹⁷ it is a good alternative to TDDFT when combined with the global hybrids. However, when using the LRC functionals, these two TD methods might end up with rather different GMH electronic couplings. Thus, when using TDA together with the LRC functionals, the FCD scheme seems to be a more reliable choice, as the Δq values are generally not affected as much by the choice of TD method as the $\Delta\mu$ values.



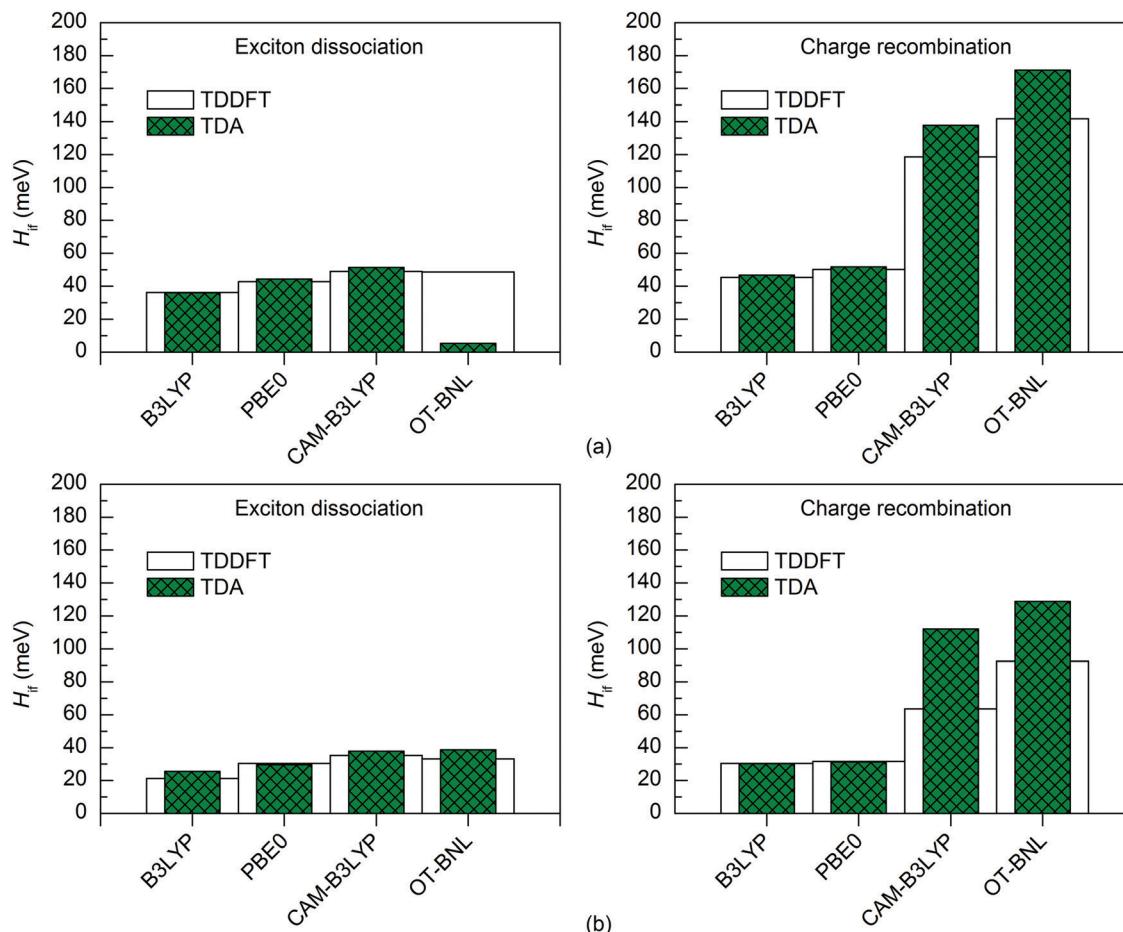


Fig. 6 Electronic couplings of (a) 3T4Q-PC₇₁BM and (b) 3Q4T-PC₇₁BM calculated with the 11-state GMH scheme using TDDFT and TDA with different functionals and the 6-31G* basis set.

Effect of the basis set

The basis set has a minimal effect on the excited state energies of the studied complexes: the vertical excitation energies are almost the same with both the 6-31G* (Table S5, ESI[†]) and 6-31G** (Table S7, ESI[†]) basis sets. With B3LYP, the 6-31+G* basis set yields only slightly (0.0–0.2 eV, Table S8, ESI[†]) smaller excitation energies for 3T4Q-PC₇₁BM than the two smaller basis sets. As this calculation was computationally already very demanding, we did not carry out the calculation for 3Q4T-PC₇₁BM at the same level of theory.

The basis set does not affect the nature of the adiabatic CT₁ and LE states much and their $\Delta\mu_{ii}^{ad}$ and Δq_{ii}^{ad} values calculated with the 11-state GMH and FCD schemes are mostly the same with 6-31G* (Tables 1 and 2) and 6-31G** (Table S12, ESI[†]). The only exception is $\Delta\mu_{CT1}^{ad}$ of 3Q4T-PC₇₁BM calculated with CAM-B3LYP, which is 0.7 D smaller with 6-31G** (15.9 D) than with 6-31G* (16.6 D), indicating a larger amount of the local component in the CT₁ state. The 6-31+G* basis set yields smaller Δq_{CT1}^{ad} of 1.6 with B3LYP than 6-31G* or 6-31G** (1.9 for both basis sets, see Tables 1 and 2 and Table S12, ESI[†]). The diabatic CT₁ and LE states determined with the 11-state GMH and FCD schemes have almost the same $\Delta\mu_{CT1}^{diab}$ and Δq_{CT1}^{diab} values with both 6-31G* (Tables 1 and 2) and

6-31G** (Table S12, ESI[†]), which indicates that both basis sets yield similar descriptions of these states. Interestingly, the Δq_{CT1}^{diab} value predicted with 6-31+G* and B3LYP does not change from the adiabatic value of 1.6 (Table S12, ESI[†]), indicating that in this case the diabatization does not remove the mixing of the local states with the CT₁ state.

The basis set has only a small effect on the 11-state electronic couplings when using the global hybrid functionals: the couplings calculated with the 6-31G* and 6-31G** basis sets (Fig. 8 and 9 and Tables S14, S15, S17, and S18, ESI[†]) differ by 0–5 meV. This is consistent with the study of Voityuk and Rösch,²⁴ in which they have presented their FCD scheme and observed that inclusion of polarization functions on hydrogen does not influence the 2-state GMH and FCD couplings of the small DNA fragments, when using HF. Here, moreover, the couplings predicted with the 6-31+G* basis set and B3LYP for 3T4Q-PC₇₁BM are only 1–2 meV larger than with 6-31G* and 6-31G** (Fig. 9 and Table S17, ESI[†]). This is also in line with the study of Voityuk and Rösch,²⁴ where the polarization functions on hydrogen and diffusion functions (on all atoms) (6-31G* vs. 6-31+G*) have been reported to have only a small (5%) effect on the couplings. Here, the smaller Δq_{CT1}^{diab} value obtained with 6-31+G* (see above) does not affect the couplings, which may be due to the compensation of other states included in

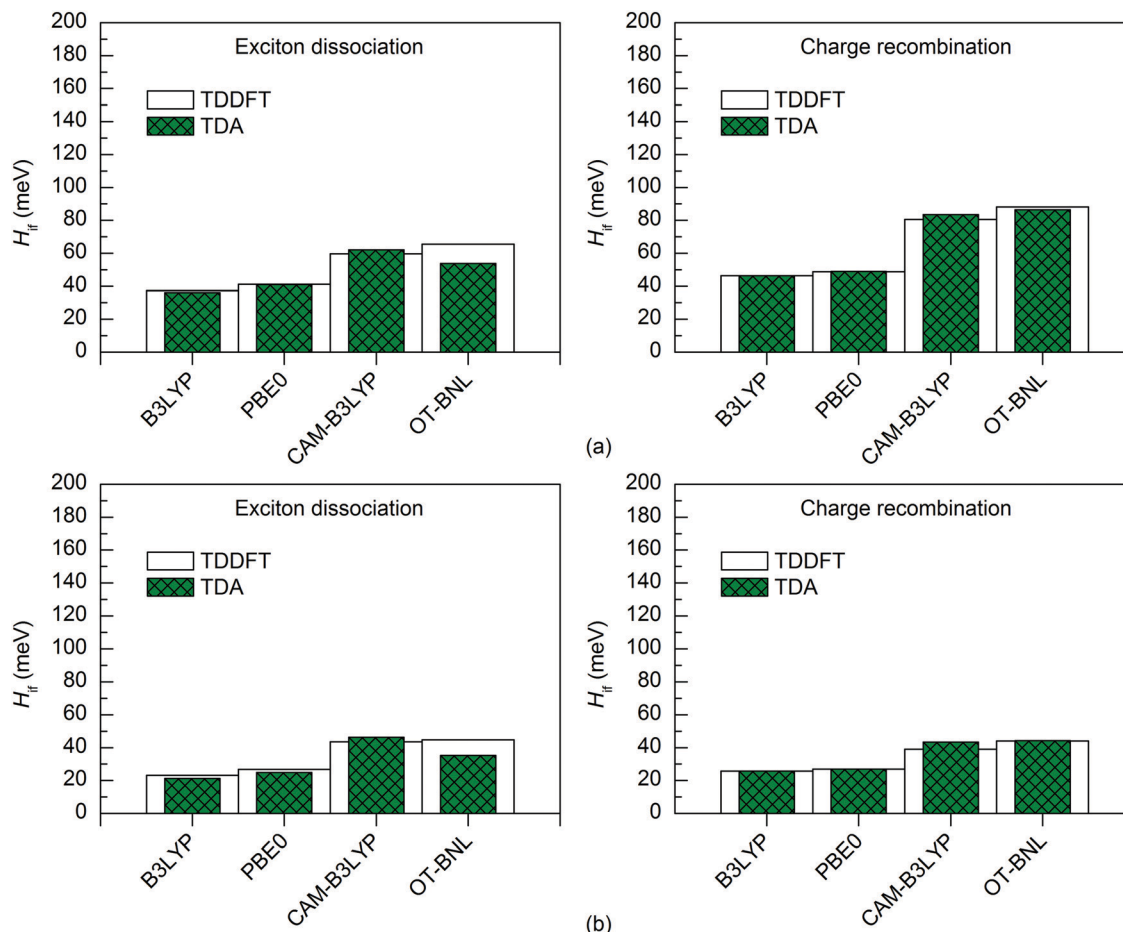


Fig. 7 Electronic couplings of (a) 3T4Q-PC₇₁BM and (b) 3Q4T-PC₇₁BM calculated with the 11-state FCD scheme using TDDFT and TDA with different functionals and the 6-31G* basis set.

the calculations. With the LRC functionals, the differences in the 11-state ED couplings predicted with two basis sets together with both the GMH and FCD schemes are also rather small, *i.e.* 0–9 meV. However, the 11-state GMH CR couplings predicted by the LRC functionals differ more, as the 6-31G** basis set yields somewhat larger (19–47 meV) couplings than 6-31G*. Generally, the 6-31G** basis set yields larger couplings in all cases, except for some PBE0 and OT-BNL values of 3Q4T-PC₇₁BM. Thus, the size of the basis set can have an effect on the dipole moments and the GMH couplings when using the LRC functionals as opposite to the global hybrids. Similar to the results obtained with different numbers of states and different TD methods, the tuning of ω does not have a notable effect on the results and both CAM-B3LYP and OT-BNL predict the same trends.

Effect of the surrounding medium

The excitation energies of the selected complexes are practically the same in different environments differing only by 0.0–0.1 eV (Tables S5, S9, and S10, ESI[†]). Thus, the polarity of the medium does not affect the adiabatic energies of the LE and CT₁ states in most cases. However, with the LRC functionals, the order of the excited states is somewhat different in 1,2-DCB and the blend from that under vacuum and the CT₁ state is at a higher

energy (the sixth or seventh state). Zheng *et al.* also observed slightly higher CT₁ state energies for the pentacene-C₆₀ complex with the OT ωB97X-D functional when using PCM compared to vacuum.⁹⁴

The nature of the adiabatic CT₁ and LE states are generally quite similar in different media (Table S11, ESI[†]). However, in some cases the portion of the LF component in the CT₁ state increases slightly in 1,2-DCB and the blend than under vacuum; namely, all functionals predict somewhat smaller $\Delta\mu_{CT1}^{ad}$ and the LRC functionals yield smaller Δq_{CT1}^{ad} . For the LE state, the $\Delta\mu_{LE}^{ad}$ and Δq_{LE}^{ad} values are mainly the same or smaller in 1,2-DCB and the blend than under vacuum, but for 3T4Q-PC₇₁BM the global hybrids predict larger values in 1,2-DCB and the blend. When comparing the diabatic states of the studied complexes obtained with the 11-state electronic coupling schemes in different media, the nature of LE states remains unchanged, and the $\Delta\mu_{LE}^{diab}$ and Δq_{LE}^{diab} values are close to zero in all the media. Moreover, the nature of the CT₁ state remains mainly unaffected by the medium polarity, although the $\Delta\mu_{CT1}^{diab}$ values of both complexes and the Δq_{CT1}^{diab} values of 3T4Q-PC₇₁BM are slightly smaller in 1,2-DCB and the blend than under vacuum. This indicates that, while the diabatic states are quite similar in the different media, the diabatization does not completely



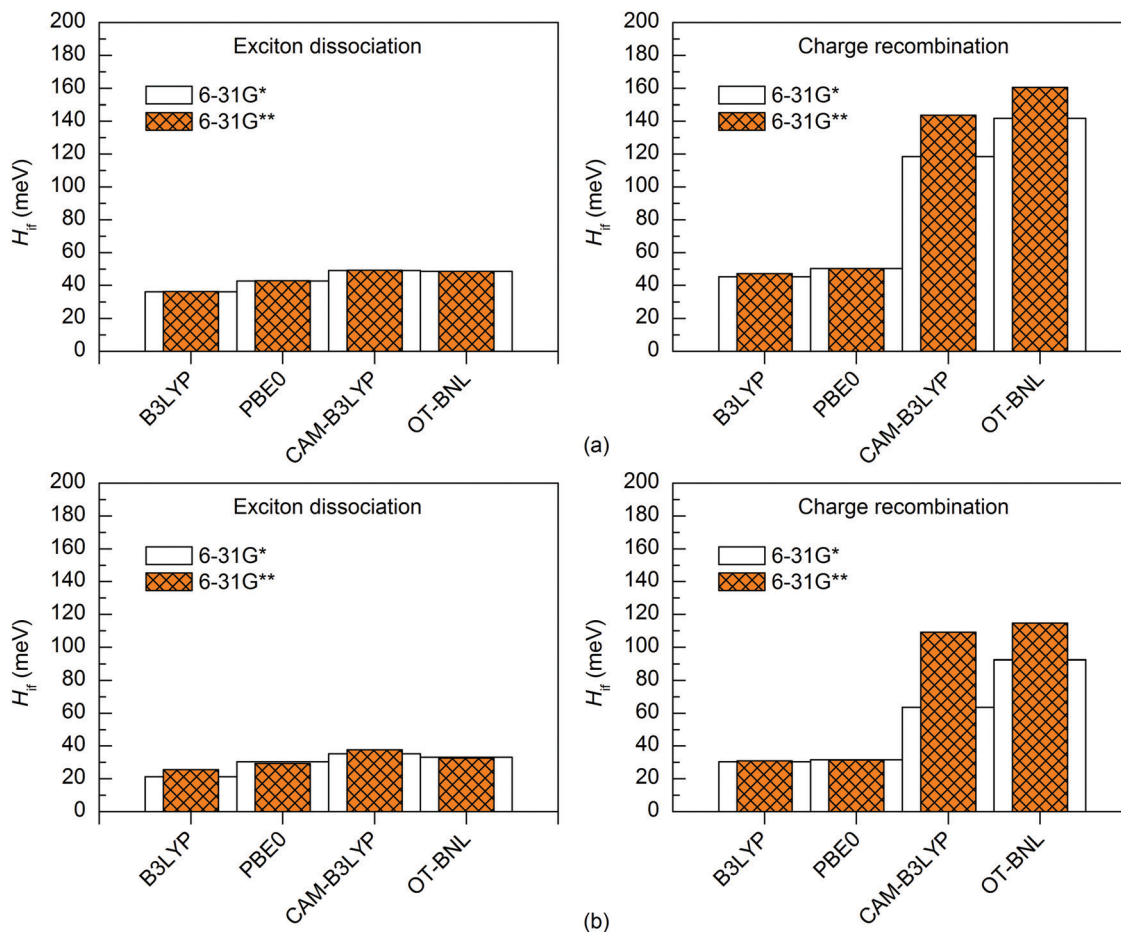


Fig. 8 Electronic couplings of (a) 3T4Q-PC₇₁BM and (b) 3Q4T-PC₇₁BM calculated with the 11-state GMH scheme using TDDFT with different functionals and basis sets.

remove the local component present in the adiabatic CT₁ state in 1,2-DCB and the blend and thus the amount of CT is slightly reduced compared to that under vacuum.

The surrounding medium has only a small effect on the 11-state electronic couplings (Fig. 10 and 11 and Tables S14, S15, S19, and S20, ESI[†]) of the complexes when using the global hybrid functionals. Moreover, the GMH and FCD results are very similar. The couplings increase only slightly (by *ca.* 0–11 meV) in the order of vacuum < blend < 1,2-DCB, *i.e.* with the increasing polarity of the medium (ϵ_s of 3.6 for the TQ-PC₇₁BM blend and 10.1210 for 1,2-DCB) in most cases. A similar trend has been observed by Lemaur *et al.* with the GMH couplings of a phthalocyanine-perylene bisimide (Pc-PTCDI) complex.⁶ With the LRC functionals, the effect of the environment on the 11-state couplings is generally also moderate (0–22 meV), but the GMH CR couplings differ more significantly, especially for 3T4Q-PC₇₁BM (by *ca.* 11–110 meV). In this case, the GMH CR couplings predicted with OT-BNL seem to be most affected by the choice of medium. Overall, the electronic couplings calculated in the different media with the LRC functionals do not follow any clear trend, although the couplings are in most cases smaller under vacuum than in 1,2-DCB or the blend. In addition, similar to that under vacuum, the 11-state FCD

couplings differ somewhat from the GMH couplings in 1,2-DCB or the blend.

Effect of the placement of PC₇₁BM on TQ

The placement of PC₇₁BM on TQ (Fig. 2b) has no effect on the vertical excitation energies and they are practically the same for both 3T4Q-PC₇₁BM and 3Q4T-PC₇₁BM (Tables S5–S7, S9, and S10, ESI[†]) regardless of the calculation method or surrounding medium. We have also observed negligible changes in the excitation energies for poly(benzodithiophene-*co*-quinoxaline)-fullerene complexes, when the orientation of PC₇₁BM is altered.⁶⁶ As the adiabatic and diabatic $\Delta\mu_{CT1}$ and Δq_{CT1} values are somewhat larger for 3Q4T-PC₇₁BM (Tables 1 and 2 and Tables S11–S13, ESI[†]), it has smaller mixing of the local LF component to the CT₁ state compared to 3T4Q-PC₇₁BM, indicating more efficient CT from TQ to PC₇₁BM.

In contrast to the vertical excitation energies, the electronic couplings are clearly affected by the placement of PC₇₁BM, as can be expected based on the previous studies of the local eD-eA interfaces of photoactive materials.^{30,31,75,76,98} The ED couplings of 3T4Q-PC₇₁BM and 3Q4T-PC₇₁BM are 36–83 meV and 21–52 meV, respectively, whereas the CR couplings are 45–252 meV and 25–150 meV, respectively (Tables S14–S20, ESI[†]).

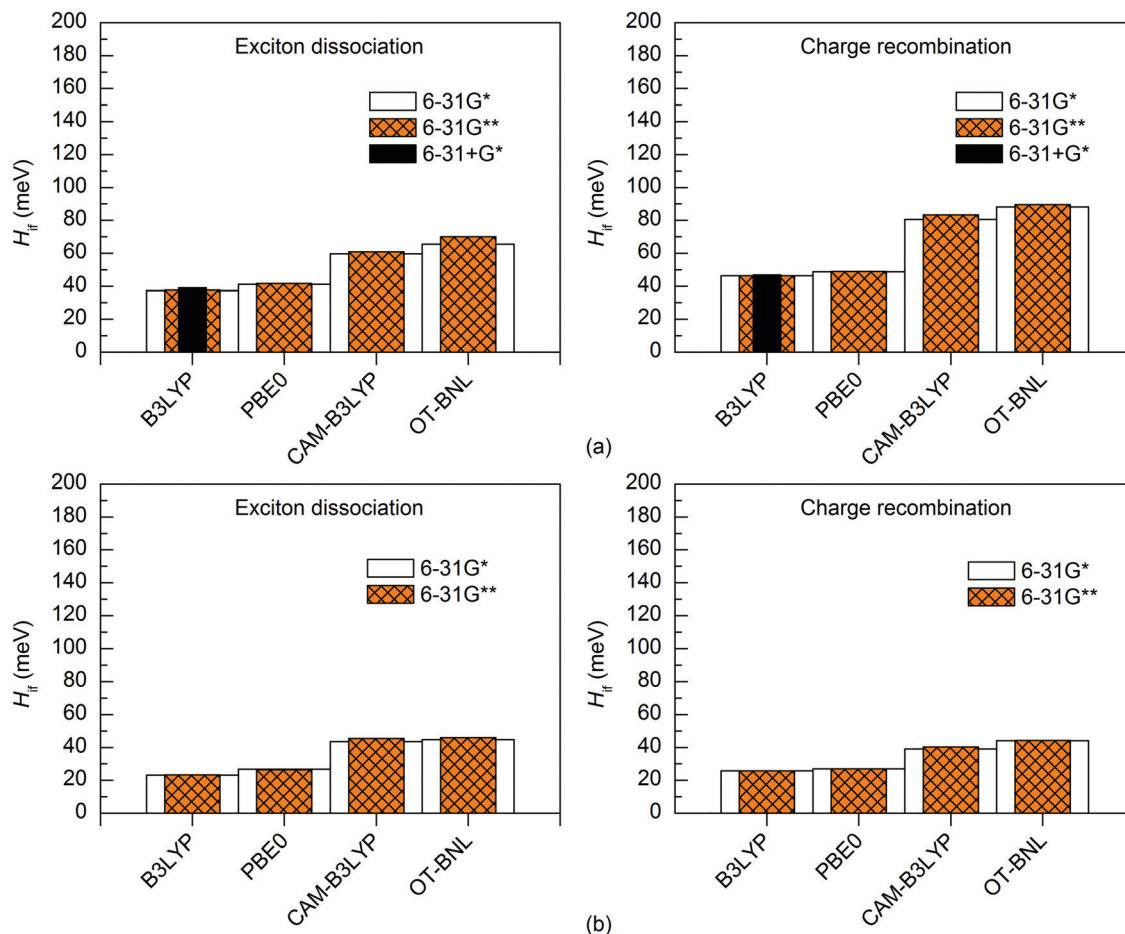


Fig. 9 Electronic couplings of (a) 3T4Q-PC₇₁BM and (b) 3Q4T-PC₇₁BM calculated with the 11-state FCD scheme using TDDFT with different functionals and basis sets.

Thus, the ED and CR couplings are *ca.* 4–30 meV and 12–132 meV stronger, respectively, when PC₇₁BM is located on the thiophene donor unit of TQ (3T4Q-PC₇₁BM) than when PC₇₁BM is on the quinoxaline acceptor unit of TQ (3Q4T-PC₇₁BM). Based on the coupling values, we anticipate faster ED and CR rates for 3T4Q-PC₇₁BM than for 3Q4T-PC₇₁BM, which is also observed from the calculated CT rates of the complexes in 1,2-DCB (see ‘Calculating charge transfer rates in 1,2-DCB and the blend’ below). For 3T4Q-PC₇₁BM, the CR couplings are larger than the ED couplings, in all cases. For 3Q4T-PC₇₁BM, the opposite, *i.e.* larger ED couplings than the CR couplings, is predicted when using the 11-state FCD scheme (and 2–4-state GMH and FCD schemes in some cases) in conjunction with the LRC functionals.

A similar effect of the relative placement on the ED and CR electronic couplings was observed by Wang *et al.* when examining 1473 complexes of polybenzo[1,2-*b*:4,5-*b'*]dithiophene-thieno[3,4-*c*]pyrrole-4,6-dione and PC₆₁BM extracted from the molecular dynamics simulations.⁹⁹ They predicted larger ED and CR coupling values when PC₆₁BM was closer to the D unit than the A unit of the copolymer, although they employed a different coupling scheme (fragment orbital approach) and functional (ω B97X-D). In their later study of a benzothiadiazole-*quater*thiophene-based copolymer with PC₇₁BM, Wang *et al.* also

observed³⁹ larger CR couplings with the 2-state FCD and the OT ω B97X-D functional when PC₇₁BM was on top of the D unit than on top of the A unit of the copolymer. Furthermore, Wang *et al.* also predicted larger couplings for the CR process than for the ED process.⁹⁹ Likewise, similar results have been obtained for the PTB7-Th-PC₇₁BM complex with the 2-state GMH³⁷ and for the α -sexithienyl-C₆₀ complex⁹⁸ with a diabatic-state approach.^{75,100} However, no clear conclusion can be drawn merely from the above findings, as opposite results have been observed, as well.^{76,98}

The differences between the electronic couplings of the two complexes are quite similar despite the calculation method (*i.e.* coupling scheme, functional, number of states, basis set, and surrounding medium), especially with the global hybrid functionals (*ca.* 4–28 meV). However, the LRC functionals predict more notable differences (7–132 meV) between the electronic couplings of 3T4Q-PC₇₁BM and 3Q4T-PC₇₁BM, especially for the CR couplings (33–132 meV).

Effect of the coupling scheme on the electronic couplings

The choice of coupling scheme has either a small or a significant effect on the coupling values of the two complexes depending on the calculation method (*i.e.* functional, basis set, and surrounding medium) used. With the global hybrids,



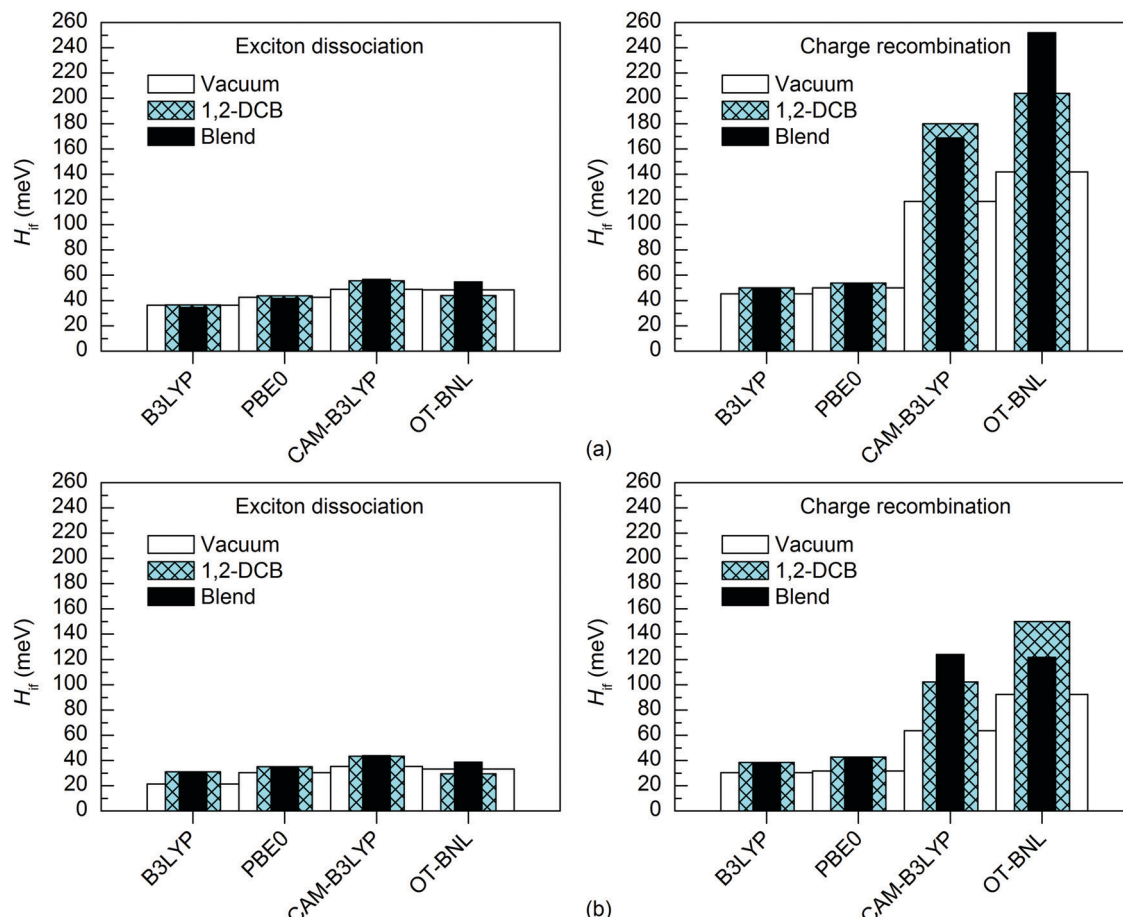


Fig. 10 Electronic couplings of (a) 3T4Q-PC₇₁BM and (b) 3Q4T-PC₇₁BM in vacuum, 1,2-DCB, and the blend calculated with the 11-state GMH scheme using TDDFT with different functionals and the 6-31G* basis set.

the 2–11-state GMH and FCD electronic couplings are quite similar despite the basis set or surrounding medium and the GMH values are only slightly (0–17 meV) larger in most cases. Moreover, both schemes predict mainly larger CR couplings compared to the ED couplings when using the global hybrids (Tables S14 and S15, ESI†), except for some FCD values of 3Q4T-PC₇₁BM calculated with PBE0 (Table S15, ESI†). With the LRC functionals, the differences (0–157 meV) between the GMH and FCD couplings are more significant compared to the global hybrids, especially in the case of the CR values. Moreover, large differences between the GMH and FCD couplings are predicted with the 6-31G** basis set (60–71 meV, in vacuum) and with the 6-31G* basis set in the 1,2-DCB or blend (61–156 meV) media. Both schemes predict larger CR couplings than ED couplings for 3T4Q-PC₇₁BM in all cases and for 3Q4T-PC₇₁BM in some cases (Tables S14 and S15, ESI†). For 3Q4T-PC₇₁BM, the 2–11-state FCD and 2–4-state GMH schemes in conjunction with the LRC functionals predict mainly larger ED couplings than the CR couplings.

Thus, the GMH scheme and more precisely the $\Delta\mu$ values employed in the GMH scheme seem to be more sensitive to the choice of functional, basis set, and surrounding medium than the FCD scheme. These findings complement the earlier

studies, which have pointed out that the Δq values in the FCD scheme are less sensitive to the mixing of the local excited and CT states, while the $\Delta\mu$ values in the GMH scheme are more affected by the mixing of the states.^{16,45} The GMH electronic couplings have been observed to improve when employing a solvent model (*e.g.* the image charge approximation, ICA), as it can lower the energy of the CT₁ state and thus decouple it from the undesired high-lying local excitations.^{16,47} However, this is not always the case, as can be seen from our results above, where the CT₁ state energies and the couplings increase somewhat in 1,2-DCB compared to vacuum. Lee *et al.* also observed relatively larger GMH couplings for a series of heptacyclo-[6.6.0.0.2⁶0.3¹³01.4¹¹0^{5,9}0^{10,14}]-tetradecane-linked D–A molecules than the FCD values with and without the ICA solvent model, when the couplings should be small due to symmetry.⁴⁵ Increasing the number of states has also resulted in improved GMH and FCD couplings.²⁸ As stated above, in this study, both coupling schemes yield very similar values despite the number of states when using the global hybrid functionals (Fig. 4 and 5 and Fig. S3 and S4, ESI†). However, with the LRC functionals, the number of states affects the couplings more, especially the CR values. With the GMH scheme, the CR values oscillate with the increasing number of states, whereas with the FCD scheme,

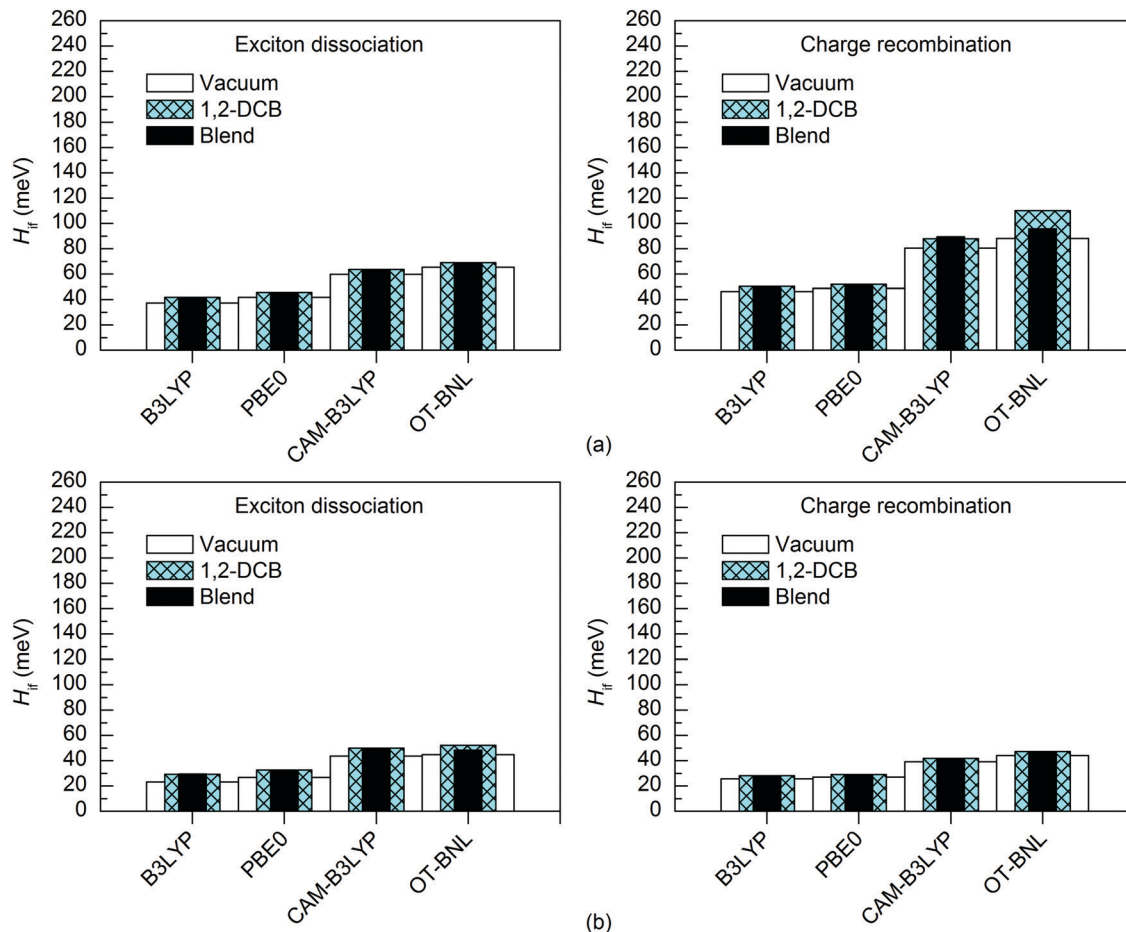


Fig. 11 Electronic couplings of (a) 3T4Q-PC₇₁BM and (b) 3Q4T-PC₇₁BM in vacuum, 1,2-DCB, and the blend calculated with the 11-state FCD scheme using TDDFT with different functionals and the 6-31G* basis set.

they decrease. Overall, the FCD scheme seems to produce couplings that are more constant and, when combined with the multi-state treatment, may be more suitable than GMH for calculating the couplings for the polymer–fullerene systems. Thus, we will employ the 11-state FCD couplings for calculating the ED and CR rates.

Calculating charge transfer rates in 1,2-DCB and the blend

Finally, we have estimated the CT rates for the ED and CR processes at the two TQ-PC₇₁BM interfaces modelled by complexes

using the 11-state FCD electronic couplings. The couplings and other parameters required for calculating the rates in both 1,2-DCB and the blend are listed in Tables 3 and 4, respectively. Generally, the inner reorganization energies (λ_i) of both complexes are smaller for the ED process than for the CR process. This can be attributed to the larger geometric changes (Fig. S5, ESI[†]) taking place in TQ during CR, *i.e.* when going from the cation geometry to that of the neutral GS ($eD^+ \rightarrow eD$), than during ED, *i.e.* when going from the S₁ geometry to that of the cation ($eD^* \rightarrow eD^+$). In other words, the geometries of the cation and the S₁ states of TQ are closer to

Table 3 Electronic couplings (H_{if})^a, internal reorganization energies (λ_i), Gibbs free energies (ΔG°), and Coulomb energies (ΔE_{Coul}) for the ED and CR processes of the TQ-PC₇₁BM complexes in 1,2-DCB with different functionals and the 6-31G* basis set

Functional	Complex	$H_{if,ED}$ (meV)	$H_{if,CR}$ (meV)	$\lambda_{i,ED}$ (eV)	$\lambda_{i,CR}$ (eV)	ΔG_{ED} (eV)	ΔG_{CR} (eV)	$\Delta E_{Coul,ED}$ (eV)	$\Delta E_{Coul,CR}$ (eV)
B3LYP	3T4Q-PC ₇₁ BM	41.9	50.3	0.1298	0.2039	-0.1373	-1.6166	-0.1373	0.1376
	3Q4T-PC ₇₁ BM	29.2	28.0	0.1308	0.2058	-0.1501	-1.5981	-0.1374	0.1372
PBE0	3T4Q-PC ₇₁ BM	48.8	52.0	0.1377	0.2180	-0.2673	-1.5951	-0.1370	0.1372
	3Q4T-PC ₇₁ BM	32.5	29.0	0.1386	0.2198	-0.2788	-1.5773	-0.1371	0.1368
CAM-B3LYP	3T4Q-PC ₇₁ BM	63.5	87.9	0.1882	0.3014	-0.3179	-1.9903	-0.1421	0.1422
	3Q4T-PC ₇₁ BM	49.9	41.7	0.1890	0.3035	-0.3139	-1.9927	-0.1421	0.1419
OT-BNL	3T4Q-PC ₇₁ BM	68.9	110.2	0.1728	0.2643	-0.2438	-1.7420	-0.1413	0.1415
	3Q4T-PC ₇₁ BM	52.2	47.1	0.1737	0.2660	-0.2479	-1.7322	-0.1419	0.1416

^a Electronic couplings obtained with the 11-state FCD scheme.



Table 4 Electronic couplings (H_{if})^a, internal reorganization energies (λ_i), Gibbs free energies (ΔG°), and Coulomb energies (ΔE_{Coul}) for the ED and CR processes of the TQ-PC₇₁BM complexes in the blend with different functionals and the 6-31G* basis set

Functional	Complex	$H_{if,ED}$ (meV)	$H_{if,CR}$ (meV)	$\lambda_{i,ED}$ (eV)	$\lambda_{i,CR}$ (eV)	ΔG_{ED}° (eV)	ΔG_{CR}° (eV)	$\Delta E_{Coul,ED}$ (eV)	$\Delta E_{Coul,CR}$ (eV)
B3LYP	3T4Q-PC ₇₁ BM	41.8	50.2	0.1423	0.2160	0.0274	-1.7451	-0.3778	0.3786
	3Q4T-PC ₇₁ BM	29.4	27.7	0.1434	0.2181	-0.0813	-1.6443	-0.4755	0.4618
PBE0	3T4Q-PC ₇₁ BM	45.5	51.9	0.1509	0.2309	-0.1006	-1.7250	-0.3770	0.3776
	3Q4T-PC ₇₁ BM	32.6	28.9	0.1519	0.2329	-0.2202	-1.6540	-0.4871	0.4322
CAM-B3LYP	3T4Q-PC ₇₁ BM	63.1	89.5	0.2067	0.3215	-0.1539	-2.1203	-0.3903	0.3907
	3Q4T-PC ₇₁ BM	49.4	41.6	0.2077	0.3232	-0.2423	-2.0818	-0.4856	0.4333
OT-BNL	3T4Q-PC ₇₁ BM	69.1	95.8	0.1871	0.2798	-0.0803	-1.8723	-0.3884	0.3889
	3Q4T-PC ₇₁ BM	48.3	47.3	0.1881	0.2814	-0.2109	-1.8090	-0.5179	0.4447

^a Electronic couplings obtained with the 11-state FCD scheme.

each other than those of the cation and GS. The contributions of the geometric changes of PC₇₁BM to λ_i are the same during the ED and CR, *i.e.* when going from the GS to the radical anion and *vice versa*, respectively. The polarity of the medium has only a minimal effect on the λ_i values, which are basically the same in 1,2-DCB and the blend. The global hybrids yield somewhat smaller λ_i values than the LRC functionals in the increasing order of B3LYP < PBE0 < OT-BNL < CAM-B3LYP. The position of PC₇₁BM on TQ does not affect λ_i much and the values are almost the same for the two complexes, λ_i of 3Q4T-PC₇₁BM being slightly larger than that of 3T4Q-PC₇₁BM, indicating slightly larger geometric changes for 3Q4T. As the accurate prediction of the outer reorganization energy (λ_s) is a rather challenging task and it is highly affected by the uncertainty of the calculated parameters,^{7,77} we have chosen to keep it as an adjusted parameter in the range of 0.10–0.75 eV. The selection of this range is based on the values of λ_s (0.11–0.50 eV) used in the previous theoretical studies of other copolymer–fullerene systems.^{33,38,77,81} We have also considered the λ_s values of 0.5–0.75 eV, because in some cases the CR rates start to compete with the ED rates in this region (see below). This region is also in line with the experimental λ of 0.22–0.8 eV^{101–103} obtained for the blends of different copolymers and fullerene derivatives.

All the functionals predict spontaneous ED and CR processes ($\Delta G^\circ < 0$) for the studied complexes, in other words, favorable processes in both media (Tables 3 and 4). Only the ED process of 3T4Q-PC₇₁BM predicted by B3LYP in the blend is not spontaneous. The experimental estimation for $-\Delta G_{ED}^\circ$ of the TQ-PC₇₁BM blend is 0.1–0.3 eV, which is obtained¹⁰⁴ as the difference between the optical bandgap of TQ (1.6–1.7 eV^{70,93}) and the CT state energy (1.4–1.5 eV^{92,93}). Thus, the calculated ΔG_{ED}° values are consistent with the experimental ones. For the selected range of λ_s (0.10–0.75 eV), all the functionals predict that ED occurs in the Marcus normal region ($|\Delta G_{ED}^\circ| < \lambda_{ED}$) in the blend. In 1,2-DCB, B3LYP and OT-BNL predict that ED takes place in the normal region for the selected range of λ_s , whereas PBE0 and CAM-B3LYP predict that ED occurs in the normal region when $\lambda_s \geq 0.14$. The CR process occurs in the inverted region of Marcus ($|\Delta G_{CR}^\circ| \gg \lambda_{CR}$) in all cases, which leads to slower CR rates than ED rates (see below).⁹ The ED and CR processes of another photovoltaic system, Pc-PTCDI,⁶ have also been observed to occur in the Marcus normal and inverted regions, respectively.

The sum of ΔG_{ED} and ΔG_{CR} is almost constant, regardless of the medium, and increases in the order of B3LYP (*ca.* 1.7–1.8 eV) < PBE0 (1.8–1.9 eV) < OT-BNL (2.0 eV) < CAM-B3LYP (2.3 eV). The constant sum indicates that the polarity of the medium does not have a significant effect on the separation between the GS and LE states.⁶ As the other energies, except that of eD* (the optimized S₁ geometry of TQ), are canceled out from the sums of ΔG_{ED} and ΔG_{CR} , the energies of eD* are consistent with the energies of the LE state (Tables S9 and S10, ESI,† S₄ for the global hybrids and S₂ for the LRC functionals). When the polarity, ε_s , increases (from 3.6 of the TQ-PC₇₁BM blend to 10.1210 of 1,2-DCB), ΔG_{ED}° and $\Delta E_{Coul,CR}$ decrease, *i.e.* become more negative, whereas ΔG_{CR}° and $\Delta E_{Coul,ED}$ increase. Lemaury *et al.* observed⁶ the same dependence of ΔG° and ΔE_{Coul} on the polarity of the medium for the modeled Pc-PTCDI complex.

The evolutions of the ED and CR rates of the studied complexes as functions of λ_s are illustrated in Fig. 12 and 13 for the 1,2-DCB and blend environments, respectively. Generally, the ED process occurs more rapidly than CR, although B3LYP, PBE0, and OT-BNL predict competing CR rates with larger λ_s (*>ca.* 0.66 eV). The ED rates are slightly faster in 1,2-DCB (10^{10} – 10^{13} s⁻¹) than in the blend (10^9 – 10^{13} s⁻¹), decreasing with increasing λ_s . Similarly, the CR rates are faster in 1,2-DCB (10^{-14} – 10^{12} s⁻¹) than in the blend (10^{-16} – 10^{11} s⁻¹), increasing with increasing λ_s . The LRC functionals predict higher ED rates compared to the global hybrids in the increasing order of B3LYP < PBE0 < OT-BNL < CAM-B3LYP. The magnitude of the ED rate predicted with B3LYP differs from those predicted with the other functionals. In the case of the CR rates, there is no clear trend between the global hybrid and LRC functionals, as the CR rates increase mainly in the order of CAM-B3LYP < B3LYP < OT-BNL < PBE0. Here, the magnitude of the CAM-B3LYP CR rate is different from that given by the other functionals. The ED and CR rates in the blend are mainly larger, when PC₇₁BM is on top of the A unit of TQ (3Q4T-PC₇₁BM) than when it is on top of the D unit (3T4Q-PC₇₁BM) (except for some CR rates predicted by PBE0 with $\lambda_s > 0.65$ eV and CAM-B3LYP with $\lambda_s > 0.4$ eV). In 1,2-DCB, 3T4Q-PC₇₁BM has larger ED and CR rates than 3Q4T-PC₇₁BM. In 1,2-DCB, both complexes have relatively similar λ_i and ΔG° values (Table 3), in which case the electronic coupling determines the rate differences between the two complexes. However, in



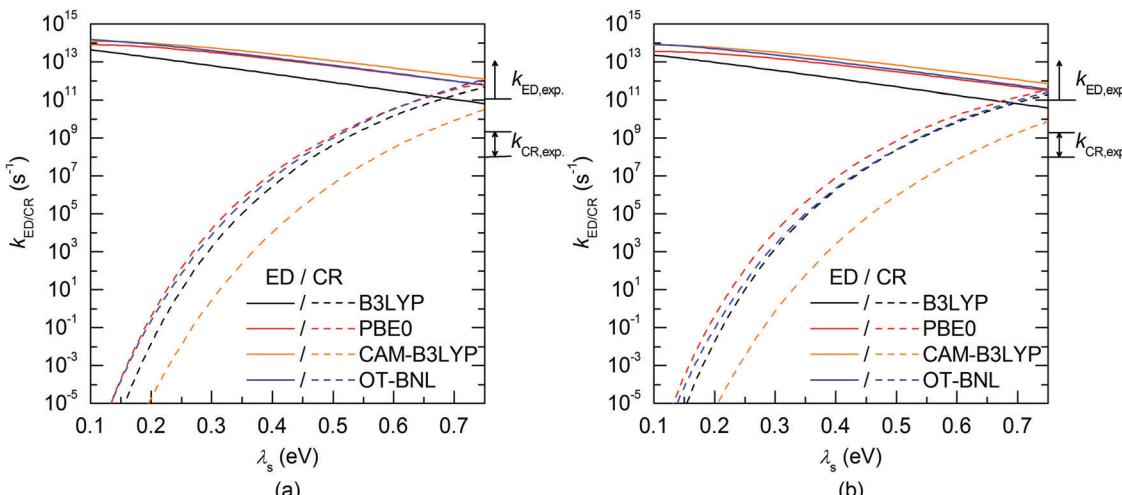


Fig. 12 Evolutions of the ED and CR rates (k_{ED} and k_{CR}) as functions of λ_s for (a) 3T4Q-PC₇₁BM and (b) 3Q4T-PC₇₁BM calculated in 1,2-DCB with different functionals and the 6-31G* basis set. The ranges for the experimental k_{ED} and k_{CR} are also shown in the figures.

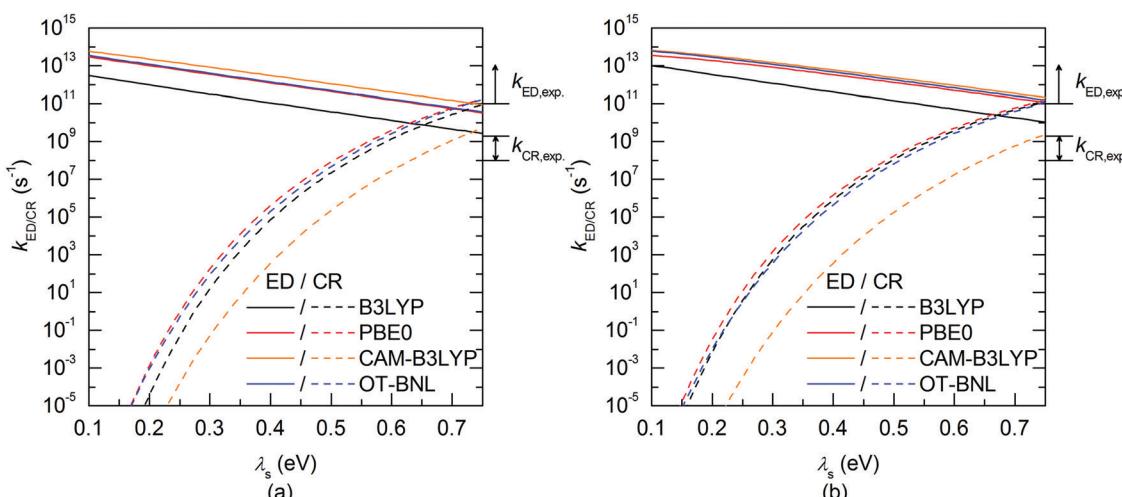


Fig. 13 Evolutions of the ED and CR rates (k_{ED} and k_{CR}) as functions of λ_s for (a) 3T4Q-PC₇₁BM and (b) 3Q4T-PC₇₁BM calculated in the blend with different functionals and the 6-31G* basis set. The ranges for the experimental k_{ED} and k_{CR} are also shown in the figures.

the blend (Table 4), the ΔG° values of the two complexes differ to such an extent that ΔG° becomes the determining factor for the rates.

The value of λ_s determines, especially in the case of the CR rates, whether the ED and CR rates are in the ranges of the experimental ED ($>10^{11}$ to 10^{15} s⁻¹ for TQ-PC₆₁BM and CR rates (*ca.* 10^8 to 10^9 s⁻¹) for different copolymer-fullerene blends. The numerical values of the CT rates at λ_s of 0.56 eV (Table 5), *i.e.* at the average of λ_s (*ca.* 0.42–0.63 eV in 1,2-DCB and 0.49–0.69 eV in the blend), for which the ED and CR rates are calculated with different functionals and in different environments are within the experimental rates. Moreover, our choices regarding the calculation methods, *e.g.* using the vacuum OT ω value in the 1,2-DCB and blend calculations or using the B3LYP geometries in all calculations, can induce some uncertainties in the calculated rates and rate parameters. However, as we have kept these computational settings consistent in all

the calculations, we expect their relative effect to be the same. To conclude, all the functionals yield mostly ED and CR rates that are consistent with the experimental ones with larger λ_s values (see above), while smaller λ_s values lead to vanishingly small CR rates.

Conclusions

We have determined the electronic couplings of the ED and CR processes at the local interfaces of solar cell materials TQ and PC₇₁BM theoretically using the two- and multi-state GMH and FCD coupling schemes. The results show that the choice of functional has the most significant effect on the excited state characteristics and the coupling values, especially with the GMH scheme. Mainly, the global hybrid functionals predict a more localized adiabatic CT₁ state, *i.e.* almost a complete CT



Table 5 Total reorganization energies (λ_{ED} and λ_{CR})^a and the rates (k_{ED} and k_{CR}) for the ED and CR processes of the TQ-PC₇₁BM complexes calculated in 1,2-DCB and the blend (in parentheses) with different functionals and the 6-31G* basis set using λ_s of 0.56 eV^b

Functional	Complex	λ_{ED} (eV)	k_{ED} (s ⁻¹)	λ_{CR} (eV)	k_{CR} (s ⁻¹)
B3LYP	3T4Q-PC ₇₁ BM	0.6898 (0.7023)	4.5×10^{11} (1.9 × 10 ¹⁰)	0.7639 (0.7760)	4.0×10^9 (3.0 × 10 ⁸)
	3Q4T-PC ₇₁ BM	0.6908 (0.7034)	2.6×10^{11} (7.5 × 10 ¹⁰)	0.7658 (0.7781)	2.0×10^9 (1.1 × 10 ⁹)
PBE0	3T4Q-PC ₇₁ BM	0.6977 (0.7109)	3.5×10^{12} (2.3 × 10 ¹¹)	0.7780 (0.7909)	1.1×10^{10} (9.3 × 10 ⁸)
	3Q4T-PC ₇₁ BM	0.6986 (0.7119)	1.8×10^{12} (7.4 × 10 ¹¹)	0.7798 (0.7929)	5.0×10^9 (1.5 × 10 ⁹)
CAM-B3LYP	3T4Q-PC ₇₁ BM	0.7482 (0.7667)	6.8×10^{12} (6.0 × 10 ¹¹)	0.8614 (0.8815)	6.2×10^7 (4.8 × 10 ⁶)
	3Q4T-PC ₇₁ BM	0.7490 (0.7677)	4.0×10^{12} (1.3 × 10 ¹²)	0.8635 (0.8832)	1.4×10^7 (3.2 × 10 ⁶)
OT-BNL	3T4Q-PC ₇₁ BM	0.7328 (0.7471)	3.7×10^{12} (2.6 × 10 ¹¹)	0.8243 (0.8398)	9.2×10^9 (5.9 × 10 ⁸)
	3Q4T-PC ₇₁ BM	0.7337 (0.7481)	2.2×10^{12} (1.0 × 10 ¹²)	0.8260 (0.8414)	2.2×10^9 (6.8 × 10 ⁸)

^a Sum of λ_i (values in Table 2) and λ_s of 0.53 eV. ^b Taken as the average of the λ_s values for which the calculated ED and CR rates are within the experimental ones (see text).

from TQ to PC₇₁BM, whereas the LRC functionals predict a small component of the intramolecular excitation of PC₇₁BM mixed with the CT₁ state. When comparing the two- and multi-state couplings, the number of states does not have a very strong effect on the coupling values with the global hybrid functionals, and the GMH and FCD couplings are quite similar. Thus, with the global hybrid functionals, the 2-state schemes seem to be sufficient for calculating the couplings of the studied system. However, with the non-tuned and OT LRC functionals, the multi-state coupling schemes yield a more localized description of the CT₁ state and thus improve couplings with respect to the two-state values. Furthermore, with the LRC functionals, the FCD scheme yields a more localized CT₁ state and constant couplings while being less sensitive to the choice of calculation method compared to the GMH scheme. Thus, the FCD scheme combined with the multi-state treatment is recommended for calculating the couplings when using the LRC functionals.

The electronic couplings are clearly affected by the position of PC₇₁BM and stronger couplings are observed when PC₇₁BM is on the donor unit of TQ than when PC₇₁BM is on the acceptor unit of TQ. In most cases, the CR couplings of the studied TQ-PC₇₁BM complexes are larger than the corresponding ED couplings. However, for the complex, where PC₇₁BM is on top of the acceptor unit of TQ, the LRC functionals predict mainly larger ED couplings. Overall, the calculated ED rates are in the range of the experimental values. However, the calculated CR values are consistent with the experimental rates only with certain values of the external reorganization energy. Nevertheless, the ED process is generally predicted to occur more rapidly than the CR process in the TQ-PC₇₁BM complexes, which is in agreement with the previous experimental results that the particular system functions efficiently in the PSCs. The slower CR rates are the consequence of the increasingly negative values of the Gibbs free energy relative to reorganization energies due to which the CR process occurs in the Marcus inverted region. We note that our study did not consider dispersion corrections, which are important for describing weak dispersion interaction in the eD-eA interface configurations, especially when determining the intermolecular distances.⁶⁶ The effect of the dispersion on the multi-state electronic couplings will be the subject of future work by our group.

Conflicts of interest

There are no conflicts to declare.

Acknowledgements

Computing resources provided by the CSC-IT Center for Science Ltd, administrated by the Finnish Ministry of Education, are acknowledged. Financing of this research by the Academy of Finland (Decision No. 251823), the Graduate School of Tampere University of Technology (TUT), the Finnish Cultural Foundation, and the Faculty of Engineering and Natural Sciences of Tampere University is greatly acknowledged by TIH and TK. ML thanks the National Supercomputer Centre (NSC), Sweden, for computing time, and the Swedish e-Science Research Center (SeRC) for financial support. The Academy of Finland (Decision No. 298182 and 310489) is acknowledged by LP for the financial support.

References

1. J. Zhao, Y. Li, G. Yang, K. Jiang, H. Lin, H. Ade, W. Ma and H. Yan, *Nat. Energy*, 2016, **1**, 15027.
2. Y. Jin, Z. Chen, M. Xiao, J. Peng, B. Fan, L. Ying, G. Zhang, X.-F. Jiang, Q. Yin, Z. Liang, F. Huang and Y. Cao, *Adv. Energy Mater.*, 2017, **7**, 1700944.
3. W. Zhao, S. Li, H. Yao, S. Zhang, Y. Zhang, B. Yang and J. Hou, *J. Am. Chem. Soc.*, 2017, **139**, 7148–7151.
4. S. Li, L. Ye, W. Zhao, H. Yan, B. Yang, D. Liu, W. Li, H. Ade and J. Hou, *J. Am. Chem. Soc.*, 2018, **140**, 7159–7167.
5. G. Yu, J. Gao, J. C. Hummelen, F. Wudl and A. J. Heeger, *Science*, 1995, **270**, 1789–1791.
6. V. Lemaur, M. Steel, D. Beljonne, J.-L. Brédas and J. Cornil, *J. Am. Chem. Soc.*, 2005, **127**, 6077–6086.
7. P. Song, Y. Li, F. Ma, T. Pullerits and M. Sun, *Chem. Rec.*, 2016, **16**, 734–753.
8. R. A. Marcus, *J. Chem. Phys.*, 1956, **24**, 966–978.
9. R. A. Marcus and N. Sutin, *Biochim. Biophys. Acta, Rev. Bioenerg.*, 1985, **811**, 265–322.
10. R. A. Marcus, *Rev. Mod. Phys.*, 1993, **65**, 599–610.
11. M. D. Newton, *Chem. Rev.*, 1991, **91**, 767–792.
12. J. L. Brédas, J. P. Calbert, D. A. da Silva Filho and J. Cornil, *Proc. Natl. Acad. Sci. U. S. A.*, 2002, **99**, 5804–5809.



13 E. F. Valeev, V. Coropceanu, D. A. da Silva Filho, S. Salman and J.-L. Brédas, *J. Am. Chem. Soc.*, 2006, **128**, 9882–9886.

14 V. Coropceanu, J. Cornil, D. A. da Silva Filho, Y. Olivier, R. Silbey and J.-L. Brédas, *Chem. Rev.*, 2007, **107**, 926–952.

15 M. Bixon, J. Jortner and J. W. Verhoeven, *J. Am. Chem. Soc.*, 1994, **116**, 7349–7355.

16 C.-P. Hsu, *Acc. Chem. Res.*, 2009, **42**, 509–518.

17 Y. Zhao and W. Liang, *Chem. Soc. Rev.*, 2012, **41**, 1075–1087.

18 J. M. Foster and S. F. Boys, *Rev. Mod. Phys.*, 1960, **32**, 300–302.

19 C. Edmiston and K. Ruedenberg, *Rev. Mod. Phys.*, 1963, **35**, 457–465.

20 T. Pacher, L. S. Cederbaum and H. Köppel, *J. Chem. Phys.*, 1988, **89**, 7367–7381.

21 Y. Mo, J. Gao and S. D. Peyerimhoff, *J. Chem. Phys.*, 2000, **112**, 5530–5538.

22 R. J. Cave and M. D. Newton, *Chem. Phys. Lett.*, 1996, **249**, 15–19.

23 R. J. Cave and M. D. Newton, *J. Chem. Phys.*, 1997, **106**, 9213–9226.

24 A. A. Voityuk and N. Rösch, *J. Chem. Phys.*, 2002, **117**, 5607–5616.

25 L. Blancafort and A. A. Voityuk, *Phys. Chem. Chem. Phys.*, 2017, **19**, 31007–31010.

26 A. A. Voityuk, *J. Phys. Chem. A*, 2017, **121**, 5414–5419.

27 Y. Shao, Z. Gan, E. Epifanovsky, A. T. B. Gilbert, M. Wormit, J. Kussmann, A. W. Lange, A. Behn, J. Deng, X. Feng, D. Ghosh, M. Goldey, P. R. Horn, L. D. Jacobson, I. Kaliman, R. Z. Khaliullin, T. Kuś, A. Landau, J. Liu, E. I. Proynov, Y. M. Rhee, R. M. Richard, M. A. Rohrdanz, R. P. Steele, E. J. Sundstrom, H. L. Woodcock III, P. M. Zimmerman, D. Zuev, B. Albrecht, E. Alguire, B. Austin, G. J. O. Beran, Y. A. Bernard, E. Berquist, K. Brandhorst, K. B. Bravaya, S. T. Brown, D. Casanova, C.-M. Chang, Y. Chen, S. H. Chien, K. D. Closser, D. L. Crittenden, M. Diedenhofen, R. A. DiStasio, H. Do, A. D. Dutoi, R. G. Edgar, S. Fatehi, L. Fusti-Molnar, A. Ghysels, A. Golubeva-Zadorozhnaya, J. Gomes, M. W. D. Hanson-Heine, P. H. P. Harbach, A. W. Hauser, E. G. Hohenstein, Z. C. Holden, T.-C. Jagau, H. Ji, B. Kaduk, K. Khistyayev, J. Kim, J. Kim, R. A. King, P. Klunzinger, D. Kosenkov, T. Kowalczyk, C. M. Krauter, K. U. Lao, A. D. Laurent, K. V. Lawler, S. V. Levchenko, C. Y. Lin, F. Liu, E. Livshits, R. C. Lochan, A. Luenser, P. Manohar, S. F. Manzer, S.-P. Mao, N. Mardirossian, A. V. Marenich, S. A. Maurer, N. J. Mayhall, E. Neuscamman, C. M. Oana, R. Olivares-Amaya, D. P. O'Neill, J. A. Parkhill, T. M. Perrine, R. Peverati, A. Prociuk, D. R. Rehn, E. Rosta, N. J. Russ, S. M. Sharada, S. Sharma, D. W. Small, A. Sodt, T. Stein, D. Stück, Y.-C. Su, A. J. W. Thom, T. Tsuchimochi, V. Vanovschi, L. Vogt, O. Vydrov, T. Wang, M. A. Watson, J. Wenzel, A. White, C. F. Williams, J. Yang, S. Yeganeh, S. R. Yost, Z.-Q. You, I. Y. Zhang, X. Zhang, Y. Zhao, B. R. Brooks, G. K. L. Chan, D. M. Chipman, C. J. Cramer, W. A. Goddard, M. S. Gordon, W. J. Hehre, A. Klamt, H. F. Schaefer, M. W. Schmidt, C. D. Sherrill, D. G. Truhlar, A. Warshel, X. Xu, A. Aspuru-Guzik, R. Baer, A. T. Bell, N. A. Besley, J.-D. Chai, A. Dreuw, B. D. Dunietz, T. R. Furlani, S. R. Gwaltney, C.-P. Hsu, Y. Jung, J. Kong, D. S. Lambrecht, W. Liang, C. Ochsenfeld, V. A. Rassolov, L. V. Slipchenko, J. E. Subotnik, T. Van Voorhis, J. M. Herbert, A. I. Krylov, P. M. W. Gill and M. Head-Gordon, *Mol. Phys.*, 2015, **113**, 184–215.

28 C.-H. Yang and C.-P. Hsu, *J. Chem. Phys.*, 2013, **139**, 154104.

29 M. H. Lee, B. D. Dunietz and E. Geva, *J. Phys. Chem. Lett.*, 2014, **5**, 3810–3816.

30 B.-C. Lin, B. T. Koo, P. Clancy and C.-P. Hsu, *J. Phys. Chem. C*, 2014, **118**, 23605–23613.

31 X.-K. Chen, M. K. Ravva, H. Li, S. M. Ryno and J.-L. Brédas, *Adv. Energy Mater.*, 2016, **6**, 1601325.

32 Z. Zheng, N. R. Tummala, Y.-T. Fu, V. Coropceanu and J.-L. Brédas, *ACS Appl. Mater. Interfaces*, 2017, **9**, 18095–18102.

33 Y. Li, T. Pullerits, M. Zhao and M. Sun, *J. Phys. Chem. C*, 2011, **115**, 21865–21873.

34 S.-B. Li, Y.-A. Duan, Y. Geng, H.-B. Li, J.-Z. Zhang, H.-L. Xu, M. Zhang and Z.-M. Su, *Phys. Chem. Chem. Phys.*, 2014, **16**, 25799–25808.

35 Y. Li, D. Qi, P. Song and F. Ma, *Materials*, 2015, **8**, 42–56.

36 Y. Li, Y. Feng and M. Sun, *Sci. Rep.*, 2015, **5**, 13970.

37 D. Qian, Z. Zheng, H. Yao, W. Tress, T. R. Hopper, S. Chen, S. Li, J. Liu, S. Chen, J. Zhang, X.-K. Liu, B. Gao, L. Ouyang, Y. Jin, G. Pozina, I. A. Buyanova, W. M. Chen, O. Inganás, V. Coropceanu, J.-L. Bredas, H. Yan, J. Hou, F. Zhang, A. A. Bakulin and F. Gao, *Nat. Mater.*, 2018, **17**, 703–709.

38 P. Song, Q. Zhou, Y. Li, F. Ma and M. Sun, *Phys. Chem. Chem. Phys.*, 2017, **19**, 16105–16112.

39 T. Wang, X.-K. Chen, A. Ashokan, Z. Zheng, M. K. Ravva and J.-L. Brédas, *Adv. Funct. Mater.*, 2018, **28**, 1705868.

40 M. Rust, J. Lappe and R. J. Cave, *J. Phys. Chem. A*, 2002, **106**, 3930–3940.

41 C. Lambert, S. Amthor and J. Schelter, *J. Phys. Chem. A*, 2004, **108**, 6474–6486.

42 A. A. Voityuk, *J. Chem. Phys.*, 2006, **124**, 064505.

43 C. Butchosa, S. Simon, L. Blancafort and A. Voityuk, *J. Phys. Chem. B*, 2012, **116**, 7815–7820.

44 A. A. Voityuk, *J. Phys. Chem. C*, 2013, **117**, 2670–2675.

45 S.-J. Lee, H.-C. Chen, Z.-Q. You, K.-L. Liu, T. J. Chow, I.-C. Chen and C.-P. Hsu, *Mol. Phys.*, 2010, **108**, 2775–2789.

46 H.-H. Chou, C.-H. Yang, J. T. Lin and C.-P. Hsu, *J. Phys. Chem. C*, 2017, **121**, 983–992.

47 H.-C. Chen and C.-P. Hsu, *J. Phys. Chem. A*, 2005, **109**, 11989–11995.

48 G. Sini, J. S. Sears and J.-L. Bredas, *J. Chem. Theory Comput.*, 2011, **7**, 602–609.

49 Z.-Q. You, Y.-C. Hung and C.-P. Hsu, *J. Phys. Chem. B*, 2015, **119**, 7480–7490.

50 A. D. Becke, *J. Chem. Phys.*, 1993, **98**, 5648–5652.

51 C. Lee, W. Yang and R. G. Parr, *Phys. Rev. B: Condens. Matter Mater. Phys.*, 1988, **37**, 785–789.

52 P. Mori-Sánchez, A. J. Cohen and W. Yang, *J. Chem. Phys.*, 2006, **125**, 201102.

53 T. Körzdörfer and J.-L. Brédas, *Acc. Chem. Res.*, 2014, **47**, 3284–3291.



54 J. P. Perdew, K. Burke and M. Ernzerhof, *Phys. Rev. Lett.*, 1996, **77**, 3865–3868.

55 J. P. Perdew, K. Burke and M. Ernzerhof, *Phys. Rev. Lett.*, 1997, **78**, 1396.

56 C. Adamo and V. Barone, *J. Chem. Phys.*, 1999, **110**, 6158–6170.

57 M. G. Medvedev, I. S. Bushmarinov, J. Sun, J. P. Perdew and K. A. Lyssenko, *Science*, 2017, **355**, 49–52.

58 P. Bleiziffer, K. Schaller and S. Riniker, *J. Chem. Inf. Model.*, 2018, **58**, 579–590.

59 M. Alipour and Z. Safari, *J. Phys. Chem. C*, 2019, **123**, 746–761.

60 T. Yanai, D. P. Tew and N. C. Handy, *Chem. Phys. Lett.*, 2004, **393**, 51–57.

61 A. E. Raeber and B. M. Wong, *J. Chem. Theory Comput.*, 2015, **11**, 2199–2209.

62 T. Körzdörfer, J. S. Sears, C. Sutton and J.-L. Brédas, *J. Chem. Phys.*, 2011, **135**, 204107.

63 L. Pandey, C. Doiron, J. S. Sears and J.-L. Brédas, *Phys. Chem. Chem. Phys.*, 2012, **14**, 14243–14248.

64 I. T. Lima, C. Risko, S. G. Aziz, D. A. da Silva Filho and J.-L. Brédas, *J. Mater. Chem. C*, 2014, **2**, 8873–8879.

65 M. Niskanen and T. I. Hukka, *Phys. Chem. Chem. Phys.*, 2014, **16**, 13294–13305.

66 T. Kastinen, M. Niskanen, C. Risko, O. Cramariuc and T. I. Hukka, *Phys. Chem. Chem. Phys.*, 2016, **18**, 27654–27670.

67 R. Baer and D. Neuhauser, *Phys. Rev. Lett.*, 2005, **94**, 043002.

68 E. Livshits and R. Baer, *Phys. Chem. Chem. Phys.*, 2007, **9**, 2932–2941.

69 T. Yamamoto, Z. Zhou, T. Kanbara, M. Shimura, K. Kizu, T. Maruyama, Y. Nakamura, T. Fukuda, B.-L. Lee, N. Ooba, S. Tomaru, T. Kurihara, T. Kaino, K. Kubota and S. Sasaki, *J. Am. Chem. Soc.*, 1996, **118**, 10389–10399.

70 E. Wang, L. Hou, Z. Wang, S. Hellström, F. Zhang, O. Inganäs and M. R. Andersson, *Adv. Mater.*, 2010, **22**, 5240–5244.

71 M. M. Wienk, J. M. Kroon, W. J. H. Verhees, J. Knol, J. C. Hummelen, P. A. van Hal and R. A. J. Janssen, *Angew. Chem., Int. Ed.*, 2003, **42**, 3371–3375.

72 Y. Kim, H. R. Yeom, J. Y. Kim and C. Yang, *Energy Environ. Sci.*, 2013, **6**, 1909.

73 E. Wang, J. Bergqvist, K. Vandewal, Z. Ma, L. Hou, A. Lundin, S. Himmelberger, A. Salleo, C. Müller, O. Inganäs, F. Zhang and M. R. Andersson, *Adv. Energy Mater.*, 2013, **3**, 806–814.

74 S. Chen, Y. An, G. K. Dutta, Y. Kim, Z.-G. Zhang, Y. Li and C. Yang, *Adv. Funct. Mater.*, 2017, **27**, 1603564.

75 Y. Yi, V. Coropceanu and J.-L. Brédas, *J. Am. Chem. Soc.*, 2009, **131**, 15777–15783.

76 L. Pandey, PhD thesis, Georgia Institute of Technology, 2013.

77 T. Liu and A. Troisi, *J. Phys. Chem. C*, 2011, **115**, 2406–2415.

78 C. W. Murray, N. C. Handy and G. J. Laming, *Mol. Phys.*, 1993, **78**, 997–1014.

79 V. I. Lebedev and D. N. Laikov, *Dokl. Math.*, 1999, **59**, 477–481.

80 S. Hirata and M. Head-Gordon, *Chem. Phys. Lett.*, 1999, **314**, 291–299.

81 C. Leng, H. Qin, Y. Si and Y. Zhao, *J. Phys. Chem. C*, 2014, **118**, 1843–1855.

82 D. A. Egger, S. Weissman, S. Refaelly-Abramson, S. Sharifzadeh, M. Dauth, R. Baer, S. Kümmel, J. B. Neaton, E. Zojer and L. Kronik, *J. Chem. Theory Comput.*, 2014, **10**, 1934–1952.

83 R. L. Martin, *J. Chem. Phys.*, 2003, **118**, 4775–4777.

84 G. A. Zhurko, *Chemcraft – graphical program for visualization of quantum chemistry computations*, Ivanovo, Russia, 2005, <https://chemcraftprog.com>.

85 P. Ros and G. C. A. Schuit, *Theor. Chim. Acta*, 1966, **4**, 1–12.

86 V. Barone and M. Cossi, *J. Phys. Chem. A*, 1998, **102**, 1995–2001.

87 M. Cossi, N. Rega, G. Scalmani and V. Barone, *J. Comput. Chem.*, 2003, **24**, 669–681.

88 A. W. Lange and J. M. Herbert, *J. Chem. Phys.*, 2010, **133**, 244111.

89 Physical Constants of Organic Compounds, in *CRC Handbook of Chemistry and Physics*, ed. J. R. Rumble, CRC Press/Taylor & Francis, Boca Raton, FL, 99th edn, 2018.

90 A. Melianas, F. Etzold, T. J. Savenije, F. Laquai, O. Inganäs and M. Kemerink, *Nat. Commun.*, 2015, **6**, 8778.

91 M. Campoy-Quiles, C. Müller, M. Garriga, E. Wang, O. Inganäs and M. I. Alonso, *Thin Solid Films*, 2014, **571**, 371–376.

92 D. H. K. Murthy, A. Melianas, Z. Tang, G. Juška, K. Arlauskas, F. Zhang, L. D. A. Siebbeles, O. Inganäs and T. J. Savenije, *Adv. Funct. Mater.*, 2013, **23**, 4262–4268.

93 A. A. Bakulin, Y. Xia, H. J. Bakker, O. Inganäs and F. Gao, *J. Phys. Chem. C*, 2016, **120**, 4219–4226.

94 Z. Zheng, J.-L. Brédas and V. Coropceanu, *J. Phys. Chem. Lett.*, 2016, **7**, 2616–2621.

95 L. Kronik and S. Kümmel, *Adv. Mater.*, 2018, **30**, 1706560.

96 G. Boschetto, M. Krompiec and C. K. Skylaris, *J. Phys. Chem. C*, 2018, **122**, 17024–17034.

97 A. Dreuw and M. Head-Gordon, *Chem. Rev.*, 2005, **105**, 4009–4037.

98 Y. Yi, V. Coropceanu and J.-L. Brédas, *J. Mater. Chem.*, 2011, **21**, 1479–1486.

99 T. Wang, M. K. Ravva and J.-L. Brédas, *Adv. Funct. Mater.*, 2016, **26**, 5913–5921.

100 T. Kawatsu, V. Coropceanu, A. Ye and J.-L. Brédas, *J. Phys. Chem. C*, 2008, **112**, 3429–3433.

101 S. Albrecht, K. Vandewal, J. R. Tumbleston, F. S. U. Fischer, J. D. Douglas, J. M. J. Fréchet, S. Ludwigs, H. Ade, A. Salleo and D. Neher, *Adv. Mater.*, 2014, **26**, 2533–2539.

102 D. C. Coffey, B. W. Larson, A. W. Hains, J. B. Whitaker, N. Kopidakis, O. V. Boltalina, S. H. Strauss and G. Rumbles, *J. Phys. Chem. C*, 2012, **116**, 8916–8923.

103 A. J. Ward, A. Ruseckas, M. M. Kareem, B. Ebenhoch, L. A. Serrano, M. Al-Eid, B. Fitzpatrick, V. M. Rotello, G. Cooke and I. D. W. Samuel, *Adv. Mater.*, 2015, **27**, 2496–2500.

104 J. Bergqvist, C. Lindqvist, O. Bäcke, Z. Ma, Z. Tang, W. Tress, S. Gustafsson, E. Wang, E. Olsson, M. R. Andersson, O. Inganäs and C. Müller, *J. Mater. Chem. A*, 2014, **2**, 6146–6152.

105 D. A. Vithanage, E. Wang, Z. Wang, F. Ma, O. Inganäs, M. R. Andersson, A. Yartsev, V. Sundström and T. Pascher, *Adv. Energy Mater.*, 2014, **4**, 1301706.

